REVIEW

Fundamentals of fluid motion in erosion by solid particle impact

J. A. C. Humphrey
Department of Mechanical Engineering, University of California at Berkeley, Berkeley, CA 94720, USA

Judging from the extensive literature on the subject, the phenomenon of material erosion by solid-particle impact continues to challenge both practitioners and theoreticians with very complex problems. Although the importance of fluid motion to this form of wear was recognized in early works, many researchers continue to interpret and attempt to understand particle impact erosion almost exclusively in terms of the material properties involved. Little attention has been given to clarifying the influence of fluid motion, especially in the turbulent flow regime. A review of some relevant issues is presented here. It starts with an exposition of the general problem and the need for better understanding. The discussion of experimental techniques is followed by various fundamental considerations relating to the motion of solid particles conditioned by the presence of a carrier fluid, neighboring particles, and a constraining solid surface. Of the experimental techniques used in erosion studies, nonintrusive optical methodologies are the most promising for measuring particle and fluid-phase velocities simultaneously near a surface. Numerical models for calculating particle-laden flows and their application to predict erosion in practical engineering flow configurations are briefly discussed. Emphasis is placed on uncovering areas of inadequate fundamental understanding of fluid mechanics phenomena that significantly affect erosion by solid particle impact.

Keywords: erosion; particles; flow; turbulent; collisions

1. Introduction

1.1 *The problem*

Surface erosion of material by solid-particle impact is a problem in nature and many multiphase flow industrial devices. Here, we are concerned with the latter, especially in the context of particle-laden gases. Figure 1 shows four flow configurations frequently encountered in engineering practice, which illustrate some of the main issues addressed in this review. The impinging jet geometry shown in Figure 1(a) spans a variety of applications, ranging from research into resistance of materials to wear to metal cutting; the boundary layer drawn in Figure 1(b) characterizes the flow over blades in turbomachinery equipment; the confined flow in Figure 1(c) occurs in the pneumatic transport of solids; and the obstructed flow for laminar and turbulent regimes in Figure 1(d) is typical of that in many heat exchangers.

The anticipated dynamic behavior of large and small particles of the same material is loosely interpreted in Figure 1. The ability of a particle to respond to changes in fluid velocity and so alter its trajectory is characterized by its momentum equilibration number, λ. It is defined algebraically by Equation 6b (later) and is the ratio of two time scales that characterize the dynamics of the solid and fluid phases, respectively. Here, we simply note that particles with $\lambda \gg 1$ are highly inertial and very slow to respond to changes in fluid velocity. In contrast, particles with $\lambda \ll 1$ faithfully follow the flow and, in principle, could be used to visualize fluid motion.

If the detailed velocity history were known for a particle that ultimately strikes a surface, we could compute the impact velocity from which the corresponding incidence angle and incidence speed would follow. Accurate measurements of impact velocity are difficult, and numerical computation is rendered highly uncertain by many of the assumptions underpinning the calculations. Notwithstanding these difficulties, the theories developed by materials scientists require knowledge of particle incidence speed and angle in order to predict surface erosion. In many past jet-blast experiments, erosive wear correlations have been based on the angle formed between the jet and the impacted surface. Many investigators have incorrectly interpreted this angle as the particle incidence angle, which has contributed to confusion in the literature.

Clearly, the magnitude of a particle's incidence velocity depends on particle–fluid, particle–particle, and particle–surface interactions as a particle approaches a surface. The characteristics of particle–fluid interactions depend on the nature of the fluid-phase flow regime (laminar versus turbulent), as well as the size, shape, relative density, and motion of the particles comprising the solid phase. Particle–particle interactions are a strong function of particle concentration and the relative motions arising from particle–surface interactions. Particle–surface interactions in turn depend on surface rebounding, surface topography, particle fragmentation, and localized thermal effects resulting from particle impacts.

There are essentially two ways of reducing undesirable erosion of material surfaces exposed to particle impacts:

(1) selection of appropriate materials for maximizing resistance to wear; and

Address reprint requests to Dr. Humphrey at the Department of Mechanical Engineering, University of California at Berkeley, Berkeley, CA 94720, USA.

Received 2 November 1989; accepted 15 February 1990

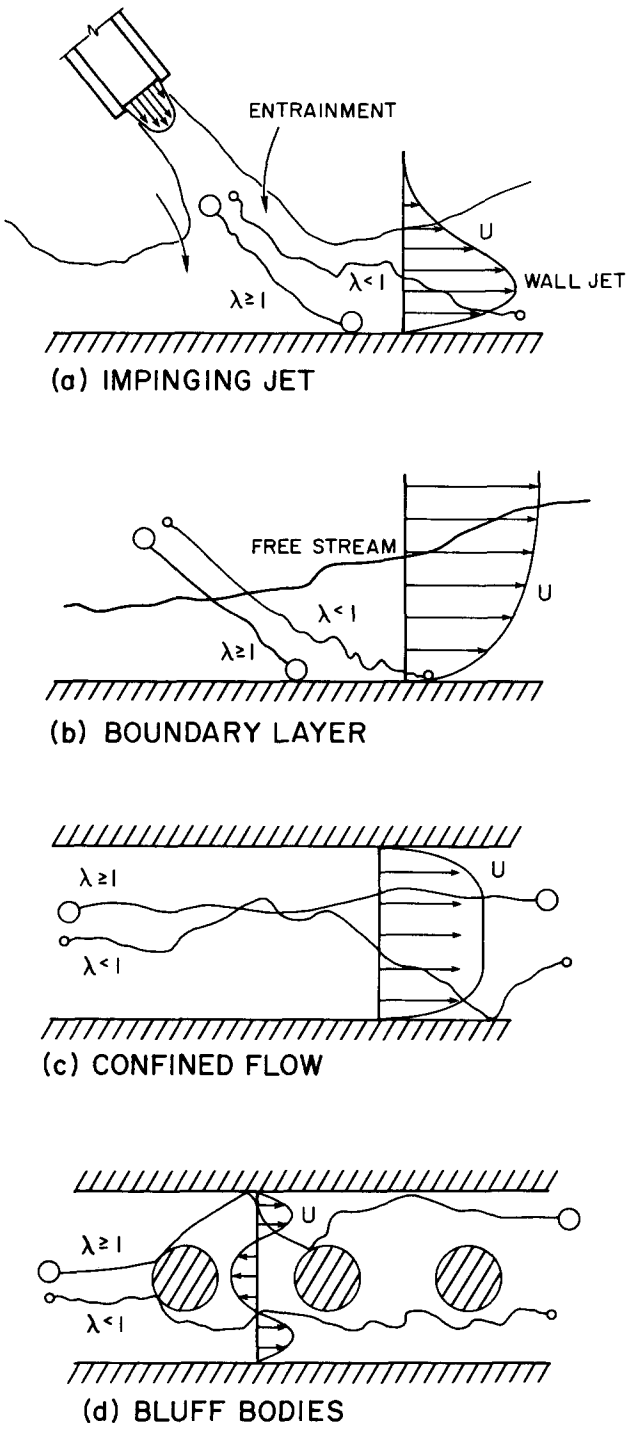

Figure 1 Examples of flow configurations prone to erosion by solid particle impact

(2) alteration of the conditions affecting fluid-suspended particle behavior, such as particle size, concentration, impact speed, impact angle, and impact location.

Much work has been done to improve the mechanical impact-wear characteristics of material surfaces. This work has led to the production of exotic, highly resistant, superalloys and ceramic materials. Unfortunately, the chemical constituents and/or the methods of production of these materials can be costly. Therefore their use is often restricted only to the most specialized or critical applications. The use of protective coatings and sacrificial surfaces has also been found to prolong the life of system components prone to erosion.[1–3] However, problems arise in obtaining good adhesion between coatings and substrates. Thus the approach is restricted to situations in which erosion-induced changes in surface shapes and their effects on the particle-laden flows can be tolerated. This method requires periodic system shutdowns and component replacements, making it expensive and/or inconvenient to implement.

The elimination of potentially erosive particles from flows wherein their presence is undesirable is the most obvious, but not the simplest, solution to the problem of erosion. Cyclones, particle separators, and filter units are examples of devices used for this purpose. Unfortunately, this approach can also be expensive and inconvenient to implement because of the periodic equipment shutdowns required for replacement of parts. In any event, complete elimination of particles of all sizes is impossible, and those that cannot be deflected or trapped may still cause damage in some systems (for example, 1–10-μm diameter coal-ash particles in large utility gas turbines). Of course, such an approach does not apply to situations in which the transport of particles is essential to the application.

Measurements of erosion, with *erosion* defined as

$$E=\frac{\text{Mass removed from a surface}}{\text{Total mass of particles impinging on a surface}}$$

show that this quantity depends markedly on the incident particle speed, V_1, and the incident angle, β_1 (the angle between a plane tangent to the surface at the impact location and the direction of motion of the incident particle). The form of the relation established empirically[4] is

$$E=kV_1^n f(\beta_1) \tag{1}$$

In Equation 1, k and n are constants assumed to depend on the physical characteristics of the materials involved, and $f(\beta_1)$ describes the dependence of erosion on the particle incidence (or impact) angle. Two commonly observed forms of this empirically determined function are shown in Figure 2—for ductile and brittle materials, respectively. Values of n for ductile materials range from 2.3 to 2.7; values for brittle materials range from 2 to 4. These ranges are approximate.

Note that, from Equation 1, altering the conditions affecting particle motion should make possible, in principle, projection

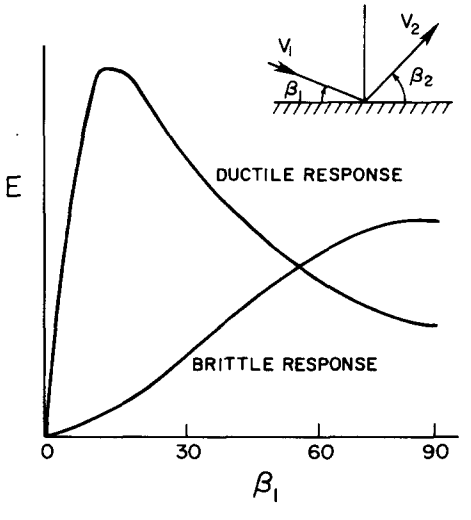

Figure 2 Typical erosion curves for ductile and brittle materials as a function of particle incidence angle, β_1, in degrees (E and β_1 are defined in the text)

of particles along less damaging trajectories. Thus control of particle trajectories and impact speeds offers a means of controlling erosion. However, such control can be achieved only if the mechanisms governing particle motion are understood and can be predicted. The mechanisms encompass a wide variety of complex physical phenomena arising from particle–surface, particle–fluid, and particle–particle interactions.

1.2 *Material versus fluid mechanics aspects of erosion*

To date, much effort has been expended researching the materials-related aspects of particle-impact erosion. By contrast, only relatively recently (since the mid-1960s) has a sustained effort been aimed at learning how to control particle erosion by *controlling particle motion*. Some of the earliest studies can be traced to erosion problems in turbomachinery components. In these studies the main objective was to correlate predictions of particle incidence speeds, incidence angles, and impact locations with surface erosion measurements for a practical range of conditions. Although various idealizations permit the detailed analysis of two-phase flows through some turbomachinery components, in many systems such an analysis is curtailed by the complexities of the flows. However, *practical* solutions to real erosion problems often do result from an improved qualitative understanding of particle–fluid motion in idealized systems.

Numerous studies of erosion of materials caused by impacting solid particles have been conducted. Examples are References 4–33, which include some fairly comprehensive reviews of the subject. Without exception, these works emphasize the materials-related aspects, and physical properties dependence, of wear in attempting to formulate physical models and mechanisms for erosion. Erosion rate differences for various substrates under similar test conditions have led to the broad classification of materials as *ductile* or *brittle*.[4,6,24] Depending on the mechanism involved, the erosion of ductile materials is further classified as *cutting* erosion or *deformation* erosion. This latter classification appears to be Bitter's[13,14] and in the early 1980s received renewed attention.[25,28,34] Although early studies focused on the analysis of single particles striking a surface, the importance of multiple overlapping impacts is now recognized and currently receives considerable attention.[11,24,25,28]

The objective of most erosion studies has been to provide information for establishing the form of Equation 1 so that, for systems with known k and n, the amount of erosion, E may be found for a given V_1 and β_1. Early studies focused on obtaining wear data in systems or equipment of practical interest for which fairly specific erosion relations were derived. Currently, assisted by the availability of more advanced measurement technology and a somewhat improved theoretical understanding of the basic mechanisms involved in erosion, the focus is on establishing more universal forms of Equation 1. Approaches are based on the interpretation of results obtained from carefully controlled experiments designed to yield fundamental and more generally applicable information. Results of such studies are summarized in References 8, 20, 29, and 31. Table 1 lists the important factors affecting erosion that have been investigated, at least to some extent.

Although not all the factors listed in Table 1 can be readily controlled or measured and although most are interrelated in a rather complex manner, distinct and sometimes quantifiable trends have emerged from their investigation. Consider, for example, the very different angular dependencies of erosion displayed by brittle and ductile materials, respectively, mentioned earlier in relation to Figure 2. Other trends revealed by experimentation, however, are inconclusive or conflicting. A case in point, discussed in some detail by Uuemois and Kleis,[20] is assessment of the influence of particle concentration. Fortunately, the conflicting evidence is explained by the relatively narrow and rather disparate ranges in particle concentration investigated in the past, which have led to very different observations and attendant interpretations. More difficult to answer with the data available are questions such as: How do particle concentration effects on erosion vary with flow conditions near a surface? Are interpretations of these effects, based on measurements made *in vacuo*, relevant to systems in which particle–surface and particle–particle interactions are potentially affected by the flow conditions near a surface?

The important point is that the behavior of a particle colliding with a surface is dependent on the particle's environment. For example, a particle that responds to part or all of the spectrum of the surrounding flow fluctuations will react differently from a particle moving in a vacuum. Similarly, the motion of a single particle will be different from that of one that collides with its neighbors. Except for the case of large inertial particles, flow conditions will affect particle concentrations and trajectories and therefore, the surface fluxes, speeds, and angles of attack that determine erosion.

From Adler's extensive review,[4] it is clear that the early recognition given to particle speed and angle of attack, as critical parameters affecting erosion, was strictly in the context of material response to particle impact. Subsequent studies, and especially *attitudes* towards the interpretation of observations, have been fixed in this mold. Thus consider a particle entrained in a fluid approaching a surface of arbitrary shape. As the particle approaches the surface, the fluid around the particle starts deviating from the particle's trajectory in order to flow along the surface. This deviation, in turn, induces a drag on the particle, which, depending on the particle's momentum

Table 1 Factors investigated that affect erosion of surfaces by solid particle impact

For particles	For surfaces	For the carrier fluid
1. Impact and rebound angles	1. Physical properties	1. State of motion (laminar versus turbulent)
2. Impact and rebound speeds	2. Change in shape caused by erosion	2. Velocity
3. Rotation before and after impact	3. Stress level	3. Temperature
4. Shape and size	4. Temperature	4. Chemical compositon and physical properties
5. Volume concentration and surface flux	5. Presence of oxide (or other) coatings	
6. Physical properties (hardness, strength, and density)	6. Simultaneous occurrence of corrosion	
7. Fragmentation		
8. Interactions (with surfaces, fluid, or other particles)		
9. Temperature		
10. Presence of additives		
11. Electrical charge		

equilibration (or inertia) number, λ, will alter its original trajectory. The component of motion of the particle toward the surface is decreased, while the component of motion parallel to the surface is increased. As a result, the particle kinetic energy varies along the particle trajectory and differs from the initial value (far from the surface) at the instant of impact.

The situation described differs totally from that in a vacuum. For systems containing fluids it is incorrect to assume that the particle's velocity at the instant of impact is equal to the surrounding fluid's velocity. Investigators frequently ignore (or overlook) this mismatch in velocities when establishing the specific form of Equation 1. The problem, as studied by Laitone,[35] is illustrated in Figure 3. Laitone's analysis shows that particles with $\lambda = 0.5$ approaching along the normal to any blunt surface *always* impinge with angles of less than 90° (except for the few particles impacting directly at the stagnation point). As a result, there is always a difference between the true incidence angle and the initial angle of a particle approaching a surface. A second finding of Laitone's analysis is that the particle incidence speed is given by the expression:

$$V_1 \propto U_f^m \tag{2}$$

where the exponent m is a function of the average fluid speed, U_f, and varies between the limits of 1 and 2.13. At very high fluid velocities, $m = 1$, regardless of the value of the inertia number, λ. As the fluid velocity is decreased, for each particle size there exists a critical fluid velocity below which $m = 2.13$. This result is important because *it affords a nonmaterials-related explanation for the fluid velocity exponents of magnitude greater than 2 observed in many ductile erosion experiments.* To obtain this result, we substitute Equation 2 into Equation 1 and, following Finnie,[8] take $n = 2$:

$$E \propto U_f^{2m} \quad \text{and} \quad 2 < 2m < 4.26 \tag{3}$$

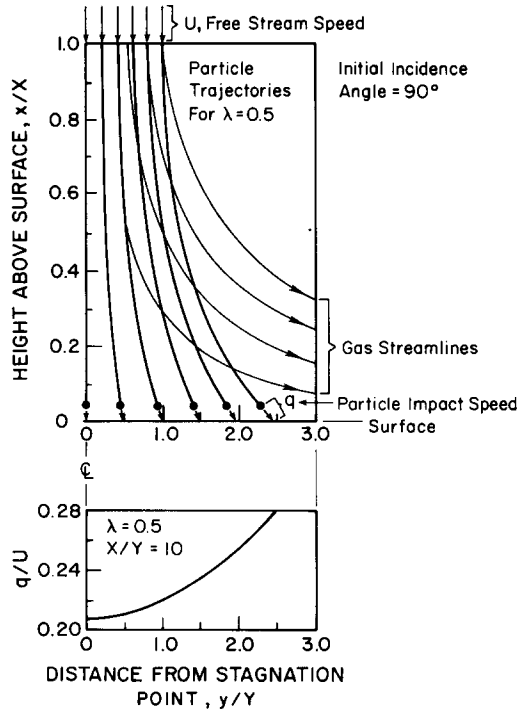

Figure 3 Gas streamlines, particle trajectories, and impact speeds for particles with a momentum equilibration number $\lambda = 0.5$ in a 2-D stagnation point flow. The particles have initial positions $0 < y/Y < 1$ and $x/X = 1$ and initially travel with the gas velocity. X and Y are characteristic lengths. Based on calculations by Laitone[35]

where, according to the analysis, the particular value of $2m$ depends *only* on U_f.

Laitone's analysis is based on the assumption of negligible interactions among particles in a streamlined flow. However, most particle-laden flows of engineering interest are turbulent, and we know[20,36] that the erosion of ductile materials decreases with the increases in particle concentration caused by particle–particle interactions. The complex dependence on fluid mechanics conditions of the net particle–surface flux in systems with significant particle–particle interactions is compounded into the experimentally determined velocity exponent $2m$.

Besides Laitone,[35,37,38] other investigators have drawn specific attention to the importance of "aerodynamic effects" in erosion. For example, the work cited in References 7 and 31 distinguishes between fluid flow conditions determining the number, direction, and speed of particles striking a surface and the mechanisms by which they actually remove surface material. Finnie[7] recognized the importance of fluid turbulence in erosion, but Dosanjh and Humphrey[39] appear to have been the first to conduct an explicit analysis. Finnie suggested that local turbulence along a roughened surface might increase erosion, although he presented no arguments to support this conjecture. Interestingly, when Dosanjh and Humphrey investigated the impinging jet configuration numerically, they found that increasing turbulence *reduces* erosion because of the enhanced radial diffusion of particles.

1.3 *Scope of this review*

The preceding fluid mechanics interpretation for the range of values observed in the exponent for velocity in Equation 1 contrasts sharply with earlier interpretations based exclusively on wear mechanisms for explaining particle–surface interactions and removal of material. For example, Tilly and Sage[19] suggested that velocity exponents of magnitude greater than 2 manifest secondary erosion caused by particle fragmentation upon impact. Finnie and McFadden[10] reexamined Finnie's cutting analysis[8] and reconsidered the assumptions concerning the location of forces during particle–surface interactions. The result was a theory that yielded better agreement between measurements and predictions of the velocity exponent. However, *both interpretations are based on considerations that exclude potentially influential fluid mechanics effects.*

The main purpose of this review is to identify and assess fluid mechanics phenomena that can significantly influence the erosion of material surfaces by impinging particles. Little is said about the actual mechanisms of erosion; excellent references addressing this topic are cited in Section 1.2. Instead, attention is focused on flow-related factors that significantly modify, or control, the wear process. These factors either change the dynamic conditions of particles approaching a surface (such as speed, impact angle, and surface flux) or change the conditions at the surface at the time of impact (temperature, roughness, deposition, rebounding, and fragmentation).

Although restricted to solid particles, much of what is said here concerning their motion also applies to liquid particles—prior to surface impaction, provided that the liquid particles are small and interactions among them are negligible. The reason for this qualification is that large liquid particles are deformed in shearing flows. Shearing can induce circulating motions inside liquid particles and, if the motions are intense, can also alter their size distribution and concentration. To explain these effects, we must consider surface tension forces. However, inclusion of such interesting but complicated phenomena is beyond the scope of this review. Schmitt[32] has documented much of the information available on erosion by liquid-particle impact.

Currently, the experimental database is inadequate for furthering a fundamental understanding of the influence of fluid mechanics, particularly turbulence, on erosion. Notwithstanding this limitation, the practical use of fluid mechanics to control particle erosion dates back to the 1940s. In 1946, Wahl and Hartstein (see Reference 6), described various German patents for the protection of bends in pipes carrying abrasive materials. The erosion of turbomachinery components also stimulated early interest in aerodynamically induced particle erosion, both in commercial and military applications. The study of erosion in highly concentrated particle–liquid flows, such as in coal slurry pipelines, has revealed additional fundamental aspects of the problem. They are very poorly understood, however, because of the more complicated particle–particle and particle–fluid interactions that occur in these non-Newtonian flows.

The problem of erosion caused by particle impact is ubiquitous and has attracted considerable attention. The abundant literature on the subject, *much of which is devoid of adequate discussions of experimental and/or numerical uncertainties*, attests to its fundamental and practical importance. Even when restricting attention to flow-related aspects of the problem in gas–solid systems, I encountered a vast amount of information, not all of which can be incorporated or even appropriately referenced in a review of reasonable length. From the sources of information available, I attempted to isolate for consideration a few of the major fundamental issues. Some of you may disagree with my choice of topics or may find that important contributions known to you are missing in this review. For these limitations I apologize in advance, hoping nevertheless that what is offered here will stimulate further thought and technical advances in this most challenging subject area.

2. Experimental techniques

The rate of erosion of a material's surface is determined by measuring the mass removed from the surface as a function of time. In the laboratory this often can be done with sufficient accuracy by weighing test specimens before and after their exposure to impacting particles. In the field, utilizing *in situ* techniques that allow remote sensing of the rate of wear is preferable. An example of the latter is the ultrasonic pulse-echo technique for monitoring wall thickness.[40]

Of special interest is separate monitoring of erosion and particle motion under carefully controlled—usually accelerated erosion—laboratory conditions. Both the time and spatial development characteristics of the wear process are important. Various erosion testers have been devised to investigate these characteristics, among which the jet-blast rig, the whirling-arm rig, and the centrifugal particle accelerator are used most often. The testers and their relative advantages and limitations are described in, for example, References 27, 28, and 41.

Although the main practical objective is to quantify and correlate cumulative wear from numerous particle impacts, we must inquire into the fundamental characteristics of single-particle impact erosion. Of particular interest are the relation of single-particle erosion to cumulative erosion and the particle–fluid dynamic conditions affecting the trajectories and speed of the particles causing erosion. Let's consider briefly several techniques that have proved particularly useful for investigating these effects.

2.1 *Characterization of surface damage and erosion*

The total amount of mass eroded from a test specimen over a period of time may be determined by simple weighing or by stylus profilometry, if sufficient mass is removed to allow precise measurement. By contrast, Andrews[42] describes a gravity-insensitive technique—based on the detection of changes in vibration frequencies—for measuring *in situ* changes of mass as small as 20 μg of specimens with total masses in the range of 0–5 g. Although more laborious, profilometry provides the spatial distribution of wear. Optical microscopy at low and high magnification and conventional metallographic techniques for examining sections through eroded specimens, used in conjunction with photography, complement the profilometry technique.[41] When very small amounts of mass removal are involved—for example, when accelerated erosion conditions are undesirable—the use of optical interferometry to quantify spatial variations in surface topography may be possible.[43]

These techniques are suitable for measuring the cumulative wear and/or wear patterns induced by large numbers of particles eroding an extended portion of a surface. Other techniques are better suited for investigating the result of single-particle impacts. Among these, scanning electron microscopy (SEM), microanalysis by X-ray spectrometry (combined with SEM), transmission electron microscopy (TEM), and selected-area electron channeling patterns (SACP) have emerged as especially useful methods.[41,44–47] SEM micrographs reveal topographic details, whereas TEM micrographs display subsurface lattice defect structures, such as dislocations, stacking faults, and twins. The SACP technique allows determination of plastic strain in and around impact sites.[44]

2.2 *Measurement of particle and fluid motion*

The techniques available for quantifying the spatial and temporal characteristics of the concentration, size distribution, and motion of a particle-laden flow can be broadly divided into mechanical and optical. The latter are nonintrusive, whereas the former must be rugged and should influence the flow minimally. Leaving aside the nontrivial problem of monitoring bulk two-phase flow conditions that guarantee statistically reproducible conditions in an experimental apparatus, of special interest is an understanding of the characteristics of the particle-laden flow in the *vicinity* of the surface undergoing erosion, particularly of the complex particle impact/rebound process.

Mechanical and nonintrusive optical techniques have been used with varying degrees of success to advance this understanding. The accuracy of mechanical methods for determining particle velocity and impact/rebound angles generally decreases with decreasing particle size and increasing particle concentration. For example, consider the rotating disk method[48] of determining the speed of particles in particle-laden erosive jet flows. Using a pair of parallel and concentric disks a fixed distance apart, rotating at a known constant angular velocity, Ruff and Ives measured the time of flight of particles passing through a radial notch in the first disk and impinging on the second. However, they did not provide details concerning particle characteristics (size, concentration, and density) in the flows tested. They recognized, but did not quantify, the disturbing effect that the rotating solid disks can induce in the jet-flow pattern. Therefore we must surmise that the technique is restricted to the measurement of speeds of fairly inertial particles ($\lambda \gg 1$) or of particles projected in a vacuum.

Among the nonintrusive optical techniques, photography has been used extensively to measure the speeds and angles of particles approaching surfaces.[49] Photographic methods include multiple-flash photography,[50,51] high-speed cameras,[52] and streaking cameras.[53] Photography can provide an impression of the phenomena occurring within a relatively large field of view, but it is expensive, labor intensive, and restricted to the plane of illumination. Additional limitations relate to the minimum particle size and maximum concentrations that can

be adequately resolved. For example, particles smaller than 25 μm and moving at high speeds are difficult to detect accurately. Some of these limitations can be relieved by using laser light sheets to illuminate the field of view as in, for example, the laser-speckle photography technique[54,55] or by utilizing laser-Doppler velocimetry (LDV), which has been described in considerable detail.[56,57]

In contrast to photography, which is a field-of-view technique, LDV allows pointwise determination of particle velocity. In this approach, if some particles are small enough that $\lambda \ll 1$, they closely follow the instantaneous fluid motion.[58] Thus by seeding a particle-laden flow with much smaller particles having good light-scattering characteristics, we can, in principle, measure both the fluid-phase and particle-phase velocities. To do so, however, we must be able to distinguish between signals emitted by small and large particles, respectively—something that can be accomplished using Doppler-signal amplitude and/or frequency discriminating techniques.[59–66] The accuracy of particle-flow velocity measurements, particle sizing, and concentration distributions using LDV and related techniques are discussed in References 67–72.

Specific applications of LDV to flows involving erosion by solid particles were reported by Tabakoff and Sugiyama.[73] They obtained statistical distributions of the tangential and normal velocity components of 0.5–60-μm ash particles striking a metal surface (unspecified) at speeds of between 72 and 96 m s^{-1}. Although their velocimeter system could not resolve the corresponding velocity components of rebounding particles, absolute values ranged between 6 and 60 m s^{-1}. Substantial differences have been observed between particle velocities determined by LDV and the rotating disk method, respectively.[49] The uncertainty of the particle-phase mean velocity was estimated to be $\pm 2.5\%$ using LDV and $\pm 18\%$ using the rotating disk method.

The potential usefulness of LDV in erosion experiments is limited by difficulties peculiar to the erosion environment. First, LDV is restricted to fairly dilute particle-laden gas flows. Second, even in dilute systems, measurements of particle velocities near a surface are subject to serious uncertainties. These uncertainties result from the finite size of the measurement volume and the need to correlate the incident characteristics of a particle with the rebound characteristics of the *same* particle. When a single particle crosses the measurement volume, resolving the directional ambiguity of the motion (i.e., distinguishing between the incident and rebound components of velocity) is necessary. In principle, this can be done using frequency shifting techniques that bias the velocity measurements. However, when particles collide (or shatter) within the measurement volume, distinguishing between their respective velocity components (or those of the fragments) may not be possible. Third, in most erosion experiments particle size is a controlled variable. Consequently, in monodisperse particle flows with eroding particle diameters larger than 10–20 μm, distinguishing between the motions of the fluid and particle phases on the basis of Doppler-signal amplitude and/or frequency discriminating techniques should still be possible. However, the distinction becomes increasingly difficult to make as the size of the eroding particles becomes smaller—approaching that of the particles following the motion of the fluid phase—which may be an important source of uncertainty in highly turbulent flows.

3. Fundamental considerations

We consider various basic issues in this section that help explain some of the difficulties facing experimental and theoretical investigations of erosive particle-laden gases. We also identify and bound the relevant problem parameters.

3.1 *Fluid motion*

The bulk of particle-laden gas flows occur in the turbulent flow regime and are characterized by irregularity, diffusivity, and three-dimensionality, all of which are guaranteed above a critical value of a characteristic Reynolds number. Although fluid turbulence is a continuum phenomenon appropriately described by the conservation equations of fluid mechanics,[74] direct numerical solutions of these equations are, for the moment, impossible to obtain for the complex configurations of engineering interest. The reason is that nonlinear terms that are responsible for the very large range of scales of motion require extensive computer storage capacity and calculation times to achieve accurate numerical solutions.

An alternative is to use a Reynolds decomposition of the field variables in the instantaneous equations and to time (or ensemble) average the result to obtain the mean-flow equations. However, this procedure generates Reynolds stresses that must be approximated as, after averaging, there are more unknowns than there are equations to solve them. Several investigators have reviewed various closure methods that proved to be especially useful to engineers.[75–80] Of these, the k–ε model[39,81–83] is of special interest. It combines a degree of accuracy for turbulent fluid flow simulation commensurate with the approximations necessary to render particle motion and erosion predictable.

3.2 *Particle motion*

Flows wherein suspended particles interact are not limited to situations involving direct physical contact of the particles. Situations arise in which—even though they do not collide (or do so infrequently)—the particles are sufficiently numerous or large that they affect one another through their collective influence on the fluid. For example, a particle passing through the wake of a larger particle, or through a cloud of particles, falls into this category. The question of averaging arises in relation to continuum (or *Eulerian*) formulations of two-phase flow transport equations and leads quite naturally to a comparative evaluation between continuum and discrete (or *Lagrangian*) theoretical descriptions of particle-laden flows. In this section we consider these issues but also call your attention to more comprehensive sources of information on the general subject of two-phase flow in References 84–100. However, you should be aware that none of these references deals specifically with the role of fluid mechanics in erosion caused by particle impact.

3.2.1 *Noninteracting particles.* Noninteracting particle motions occur when the dynamics of any one particle are not influenced by the presence of neighboring particles (either directly, through collisions, or indirectly, through the perturbed fluid field). The conditions for this phenomenon correspond to fairly dilute systems characterized by volume fractions α (volume of solids/total volume) of less than 10^{-3} and mass loading ratios γ (mass of solids/total mass) of less than 1 for particle–fluid systems with pure phase-density ratios of $\rho_p/\rho_f \simeq 10^3$. Typically, then, interparticle distances are on the order of $20 \times d_p$ or greater,[98] where d_p is the effective (spherical equivalent) diameter of a particle.

The general Lagrangian equation of motion for a single particle in arbitrary accelerated motion is given, by Clift *et al.*,[97] who discuss its derivation and solution. For the

condition that $\rho_p/\rho_f \gg 1$, the equation is

$$\frac{du_{pi}}{dt}=\left(\frac{3\rho_f C_D}{4d_p\rho_p}\right)(u_{fi}-u_{pi})|\vec{u}_f-\vec{u}_p|+g_i \tag{4}$$

where $i=1, 2$, and 3 are the three cartesian coordinate directions, and instantaneous velocity components for the particle, u_{pi}, and the fluid, u_{fi}, are implied. In Equation 4, $|\vec{u}_f-\vec{u}_p|=|\vec{u}_r|$ is the modulus of the instantaneous relative velocity of the particle, and g_i is the i component of gravity. For the particle drag coefficient, C_D, empirical relations covering a wide range of particle Reynolds number are frequently used. Thus, for example, Rudinger[98] suggests that

$$C_D=\frac{24}{\mathrm{Re}_p}(1+\tfrac{1}{6}\mathrm{Re}_p^{2/3}) \qquad 0\leqslant \mathrm{Re}_p \leqslant 500 \tag{5}$$

where $\mathrm{Re}_p=|\vec{u}_r|d_p/\nu$ is the particle translational Reynolds number based on the modulus of the instantaneous relative velocity, particle diameter, and fluid kinematic viscosity, ν.

The drag coefficient given by Equation 5 was obtained experimentally for smooth spheres in streams of uniform flow with low turbulence intensity. However, in many systems the relative flow past a particle is turbulent because of preexisting time and length scales of motion. When these scales are commensurate with those of the particle, the turbulence modifies the instantaneous flow field around the particle and hence the net drag, which will differ from that predicted by Equation 5. Experimental relations are available that explicitly account for the effect of turbulence structure on the drag coefficients for spheres. Turbulence-dependent coefficients for subcritical, critical, and supercritical flow conditions as a function of the free-stream relative turbulence intensity are tabulated in Reference 97. In principle, these correlations could be used in Equation 4 to calculate $\vec{u}_p$.

Rarely, however, is the instantaneous fluid velocity, $\vec{u}_f$, in Equation 4 known for turbulent flow configurations of practical interest. More likely, the mean velocity, $\vec{U}_f$, will have been determined experimentally or by numerical computation, utilizing a turbulent model. Ensemble averaging of the terms in Equation 4—subject to the assumption that the instantaneous velocities $\vec{u}_f$ and $\vec{u}_p$ can be Reynolds decomposed into means $(\vec{U}_f, \vec{U}_p)$ plus fluctuations $(\vec{u}'_f, \vec{u}'_p)$—yields an equation for the mean particle velocity, $\vec{U}_p$. This equation depends on $\vec{U}_f$ and on a separate, rather complicated term that accounts explicitly for the correlations among the velocity fluctuations. The correlations account for the so-called turbulence drift velocity[101] caused by turbulent diffusion, which is frequently calculated using a flux or gradient model approximation. An alternative to modeling the drift velocity is to calculate $\vec{u}_p$ directly from Equation 4 using $\vec{u}_f=\vec{U}_f+\vec{u}'_f$ for the instantaneous fluid velocity, where the fluctuation is determined and added to the mean velocity according to some rule. Then, the mean particle velocity, $\vec{U}_p$, if required, must be found by averaging over several realizations of the computed flow. Direct determinations of $\vec{u}_p$, subject to rules for $\vec{u}_f$ that preserve the basic character of the turbulent motion, have been performed.[83,102–104]

The assumptions embodied in Equation 4 are: (a) quasi-steady motion of noninteracting spherical particles; (b) negligible virtual mass, pressure gradient, Basset, Magnus, and Saffman forces; and (c) the only body force is that of gravity. The accuracy of assumptions (a) and (b) are discussed by Rudinger[98] who concludes that, except for the neglect of the Basset history term, the assumptions are justified in particle-laden gas flows. For density ratios of $\rho_p/\rho_f > 10^3$, Rudinger shows that the Basset force becomes smaller than 10% of the Stokes drag for times larger than $\frac{1}{2}\tau_p$, where τ_p is the characteristic particle relaxation or response time:

$$\tau_p=\frac{\rho_p d_p^2}{18\mu f_D} \tag{6a}$$

in which μ is the fluid viscosity and $f_D=\mathrm{Re}_p C_D/24$. If τ_p is made nondimensional by a characteristic flow time scale, such as $\tau_f=L_c/|\vec{U}_{fc}|$, where L_c and $|\vec{U}_{fc}|$ are a characteristic length and a mean fluid velocity scale, respectively, the *momentum equilibration* number, λ, is defined as

$$\lambda=\frac{\tau_p f_D}{\tau_f} \tag{6b}$$

For $f_D=1$, corresponding to creeping flow, λ becomes identical to the "inertia" or Stokes number, $\mathrm{St}=\tau_p/\tau_f$. In this review we use the two names for λ interchangeably, its precise value being determined by Equation 6b.

Although neglecting Magnus and Saffman forces may be reasonable in the bulk of a flow, at solid surfaces where particles can rebound with large angular velocities and near which regions of strong fluid shear are induced the magnitudes of these terms may be significant relative to the drag term. Even in the bulk of the flow, if the turbulence fluctuations are intense, Saffman forces can alter particle trajectories and induce corresponding large-scale flow inhomogeneities.[93]

For a prescribed variation of the fluid velocity components, u_{fi}, the numerical solution of Equation 4 is readily achieved using a Runge–Kutta integration technique. The trajectories of a particle can be found from its velocity components:

$$\frac{dx_i}{dt}=u_{pi} \tag{7}$$

Knowledge of particle speeds and trajectories makes possible extrapolation of incidence speeds and angles at the impact locations.[35,37–39,83] From the incidence values, erosion may be determined with an appropriate wear model.[39,83]

3.2.2 *Interacting particles.* The dynamics of interacting particle flows have been the subject of indepth research.[87–89] Calculations based on the theories proposed by Yeung[105] and Abrahamson[106] suggest that, for mass loading ratios $\gamma<1$ $(\alpha<10^{-3})$ of particle–gas systems with $\rho_p/\rho_f \simeq 10^3$, particle–particle collisions are infrequent. However, for these conditions the average interparticle distance is less than 20 times d_p. In turbulent flow, this distance may not be sufficient to rule out *indirect* interactions among particles, especially in regions where large slip velocities occur between the two phases. For conditions under which the motion of the particle phase affects the motion of the fluid phase (two-way coupling), the two motions must be calculated simultaneously.[107,108]

In considering indirect particle interactions, Hinze[93] distinguished among: (a) effects of the increased effective shear rates in the fluid; (b) effects of the wakes of particles with large relative velocities; (c) effects on turbulence intensity, integral scale, eddy diffusivity, and viscous dissipation of the fluid because the fluid occupies less space; and (d) clustering of particles, which on the scale of the clusters may modify the fluid flow pattern. Associated with (a) and (b) are modifications to the energy spectrum of the fluid in the wave-number ranges corresponding to the average interparticle distance and the particle diameter, respectively. These modifications imply increasing fluid-phase dissipation rates with increasing particle concentrations, which is in agreement with experimental measurements and theoretical analyses performed for dilute systems.

In principle, we should be able to extend the form of Equation 4 to include acceleration terms arising from direct and indirect

particle interactions, respectively. For example, numerical simulations of the air flow of 10-μm and 210-μm alumina–silica particles through a venturi meter show that the inclusion of direct particle–particle interactions significantly alters the predicted characteristics for $\gamma > 2$, as a result of the momentum exchanges between the two phases.[109] The model used for direct interactions contains the assumption of elastic collisions among particles and neglects multiple scattering.[90] The form of the interaction term is complex and, although there is no direct evidence of its validity, its inclusion in the numerical formulation improved the agreement between measurements and calculations of pressure drop and pressure recovery through a venturi meter for mass loading ratios of $\gamma > 2$.

In flows having strong particle interactions, the use of standard (single-sphere) drag coefficient relations is inappropriate, and modified drag coefficients are required.[98] Because of the complexities involved, we must rely on experimental measurements of the coefficients for specific configurations and flow conditions of interest. Unfortunately, the associated experimental uncertainties are rather large.

3.2.3 *The effects of turbulence.* Considerable information pertaining to the influence of turbulence on particle motion, particularly in relation to particle dispersion in the bulk of a fluid, is available. By contrast, little information is available regarding how the presence of a surface (a) alters the dispersion mechanism(s); (b) changes the particle flux to the surface; and (c) influences the evolution of the wear patterns observed as a result of evolving surface topography. Among others, Owen[92] and Hinze[93] considered some fundamental aspects of turbulent fluid–particle interactions. Here, we briefly summarize the most relevant findings in these and some related investigations.

Hinze[93] investigated the response time of a discrete spherical particle relative to the various characteristic times of the turbulent carrier fluid. Among his major conclusions were that particles with $d_p/\eta \leq 1$, where η is the Kolmogoroff (dissipative) microscale of turbulence, will respond to the motion of the smallest eddies. The approximate condition for this response is

$$\frac{d_p}{\eta} < \left(\frac{10}{\rho_p/\rho_f + \beta}\right)^{1/2} \tag{8}$$

where β is a coefficient of order unity related to the virtual mass contribution to the particle momentum balance. For sand in air ($\rho_p/\rho_f \sim 2{,}000$) this condition gives $d_p/\eta \simeq 0.1$. In a typical turbulent flow at a high Reynolds number, $\eta \simeq 10$–$100\,\mu$m, implying that particles with $d_p < 1$–$10\,\mu$m will respond to this scale of motion. By contrast, the condition necessary for particles of the same density ratio to adapt to the motions of the large energy-containing eddies, say of size ℓ, is

$$\frac{d_p}{\ell} < \left(\frac{\nu/\tilde{u}_f \ell}{\rho_p/\rho_f + \beta}\right)^{1/2} \tag{9}$$

where the tilde in $\tilde{u}_f$ denotes the rms component (or some related characteristic measure) of the turbulent fluid velocity. For the case of sand in air flowing through a 20-in. (0.5-m) diameter pipe, typically $\nu/\tilde{u}_f \ell < 100$ and Equation 9 yields $d_d < 10^{-3}$ m. Thus heavy particles larger than 1 mm in diameter will be relatively insensitive to all scales of turbulent motion in air.

These results clearly indicate that many industrial particle-laden flows can contain a range of particle sizes and flow conditions capable of satisfying Equation 9 but not Equation 8. These particles do not experience the full spectrum of turbulence, and we anticipate considerable difficulty in attempting to model the influence of turbulence on their motion.[93,110]

For particle suspensions with $\rho_p/\rho_f \gg 1$, the Magnus force induced by particle rotation is generally small. By contrast, particles with $d_p/\eta \leq 1$ immersed in the thin shear layers that can develop between eddies may experience a large lateral force that drives them through the shear layers during the life of the eddies. This force is referred to as the Saffman force. It can induce clustering of particles within eddies, where shear rates are lower, and promote large-scale concentration fluctuations that affect the turbulence characteristics of the suspension. We discuss Magnus and Saffman forces in more detail in Section 3.3.3 for particles rebounding from surfaces.

For long diffusion times, analyses of particle motion must allow for the possibility that the particle will escape from the fluid surrounding it originally. Most theoretical analyses yield $\nu_p/\nu_f < 1$ for the ratio of particle-phase to fluid-phase eddy diffusion coefficients, but this result is at variance with experimental evidence[111,112] and numerical calculations,[110,113,114] which show that for large, dense particles it is possible to find a $\nu_p/\nu_f > 1$. Theory predicts that ν_p/ν_f increases markedly when the particle size becomes on the order of, or larger than, the Taylor microscale, λ_T.[111] Because $\eta \ll \lambda_T \ll \ell$, this prediction suggests a filtered response of the particles to the spectrum of fluid turbulence.

Owen[92] also investigated the effects of particles on the turbulence of a gas phase relative to the pneumatic transport of particles through horizontal pipes. For dilute systems of small particles in a Stokes flow regime, he showed that the dissipation of turbulent kinetic energy by the fluid phase in a pipe flow at fixed Reynolds number increases with increasing particle concentration. A related result is that the ratio of characteristic gas-phase velocity fluctuations with and without small particles present should vary according to

$$\frac{\tilde{u}_{f,p}}{\tilde{u}_f} \simeq \left(1 + \frac{\alpha \rho_p}{\rho_f}\right)^{-1/2} \tag{10}$$

Assuming that the turbulent length scale ℓ is not affected by the presence of the particles, the ratio of eddy-diffusion coefficients for fluid with and without particles, $\nu_{f,p}/\nu_f$, should also vary according to Equation 10. The result is a reduced eddy-diffusion coefficient of fluid with particles relative to fluid without particles.

Extension of Equation 10 to apply to larger particles prone to turbulence-spectrum filtering effects yields

$$\frac{\tilde{u}_{f,p}}{\tilde{u}_f} \simeq \left[1 + \left(\frac{\alpha \rho_p}{\rho_f}\right)\left(\frac{\tau_e}{\tau_p}\right)\right]^{-1/2} \tag{11}$$

where τ_p is given by Equation 6a and $\tau_e\,(\equiv \ell/\tilde{u}_f)$ is the characteristic time of an energy-containing eddy.

In considering how particles in pipe flow are projected toward a wall, Owen proposed that the particles are convected from regions of intense turbulence outside the viscous sublayer by occasional eddies that penetrates the sublayer. In terms of particle dynamics, Owen divided the wall flow region into two layers. Away from the wall, particles are dispersed (in a direction normal to the wall) by the action of turbulent diffusion, leading to the name *diffusion regime* layer. Near the wall, the particles are convected instead, hence the term *convection regime* layer. Within the diffusion layer, $\tau_p/\tau_e < 1$, but within the convective layer $\tau_p/\tau_e \geq 1$. (Near the wall a more appropriate estimate for τ_e is ν/u_τ^2, where $u_\tau = (\tau_w/\rho_f)^{1/2}$ is the friction velocity at the pipe wall, τ_w being the wall shear stress.)

Rizk and Elghobashi[115] analyzed the influence of a plane wall on the motion of spherical particles suspended in a turbulent fluid. Their study extended Chao's earlier work,[116] in which he treated the Lagrangian equation of particle motion as a linear, stochastic integro-differential equation, to which he applied the Fourier transform. Rizk and Elghobashi extended Chao's formulation to account for the additional wall-induced drag on a particle and the Saffman lift force resulting from shear. They obtained expressions that relate the turbulence

intensity, energy spectrum, and double-velocity correlation coefficient of the two phases. Their results apply to particles smaller than the dissipative scale of motion for which both $Re_p \ll 1$ and $Re_s \ll 1$, where Re_p is the particle translational Reynolds number previously defined, and $Re_s = d_p^2 \Omega_f / \nu$ is the particle shear Reynolds number based on the modulus of the fluid vorticity vector, $\tilde{\Omega}_f$. Their main conclusions were that in the vicinity of a wall: (a) turbulent fluid fluctuations are more strongly damped than turbulent particle fluctuations; (b) the rms velocity of a particle near a wall is greater than that of a particle removed from the wall, particularly in the direction normal to the wall to which the shear lift force contributes strongly; (c) the relative influence of the lift force on particle motion extends farther from the wall than the additional viscous drag; and (d) a particle's response to turbulent fluid fluctuations decreases with increasing particle size and density. Rizk and Elghobashi provided closed-form expressions for the wall–distance dependence of their observations. The Fourier transform methodology developed by Chao allowed them to find expressions of the form:

$$\left(\frac{\widetilde{u_{pi}}}{\widetilde{u_{fi}}}\right)^2 = \int_0^\infty \Omega F(\omega)\, d\omega \qquad (12)$$

which relate the turbulence intensity of the particle motion to that of the surrounding fluid through the fluid's energy spectrum, $F(\omega)$, and the ratio of two polynomials, Ω, which depends on flow fluctuation frequency, particle fluid density ratio, and distance from the wall.

Figure 4[115] shows normalized particle and fluid rms velocities parallel and normal to a wall as a function of the dimensionless wall distance $y^+ = yu_\tau/\nu$. The calculations are for $\rho_p/\rho_f \simeq 1{,}500$, which corresponds roughly to coal particles in air at 25°C. As for y, the particle sizes were normalized by ν/u_τ. The dots in the figure correspond to measurements of pure fluid-phase fluctuations,[117] with which the authors obtain agreement for $d_p^+ \leq 0.02$.

Qualitative confirmation of many of the findings presented in this section are reported for numerous experiments performed in particle-laden jets and pipe flows.[66,82,104,118–121] Boothroyd and Walton[120] reported that fluid turbulence and its mean velocity gradient were markedly reduced by particles near a wall in pipe flow. Impinging particles accounted for a large fraction of the wall shear stress and the attendant observed reduction in the friction factor. References 66 and 121 show that laser-Doppler measurements provide a clear impression of the response of the mean and fluctuation flow components to particle size and concentration. Tsuji *et al.*[66] investigated the flow of particle-laden air through a vertical pipe. Flows with particles ranging in size from 200 μm to 3 mm were investigated at pipe Reynolds numbers of approximately 2.2×10^4. In general, over a pipe cross section, large particles increased air turbulence, whereas small particles reduced it. Both effects varied in direct proportion to particle concentration. Increases in turbulence were most noticeable in the core of the flow, and decreases were marked near the pipe wall. Intermediate particle sizes (500 μm) showed both effects simultaneously.

In summary, despite considerable work, a small sample of which we have discussed, a wide gap persists between the qualitative and quantitative understanding of the effects of turbulence on particle motion in two-phase flow. Most of the trustworthy quantitative information available for particle-laden gases pertains almost exclusively to dilute systems of small particles away from walls. The important constraints imposed by the presence of solid surfaces in the flow—and the implications for erosion—remain undocumented and poorly understood. Theoretical attempts to model turbulence effects on particle motion rely either on experimentally determined drag

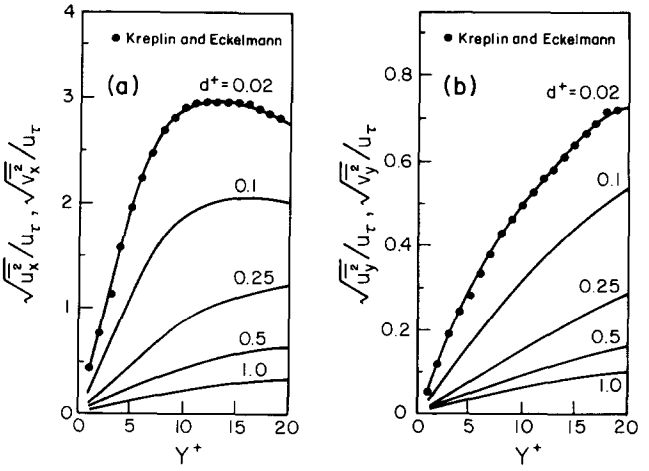

Figure 4 Fluid (u, dots) and particle (v, lines) rms velocities parallel (x component) and normal (y component) to a wall for a particle/fluid density ratio $\rho_p/\rho_f = 1{,}500$ and different dimensionless particle sizes, d^+. Conditions correspond to a dilute suspension of spherical particles in a fully developed turbulent channel flow with Re = 7,700. Based on calculations by Rizk and Elghobashi[115] and measurements by Kreplin and Eckelmann[117]

correlations that are prone to serious uncertainties or on *ad hoc* extensions of formulations premised on considerations relating to single particles. Even for gas–solid systems, in which the condition $\rho_p/\rho_f \gg 1$ simplifies the particle equation of motion considerably, analytical solutions are few. Instead, we must rely on numerical methods to calculate particle speeds and trajectories.

3.2.4 *Lagrangian versus Eulerian descriptions of particle motion.* A Lagrangian description of particle motion implies a discrete particle phase. An Eulerian description treats the particle phase as a continuum that permits appropriate definitions of averaged field quantities. Both approaches are reported extensively in the literature.

The Lagrangian approach predicts the speeds and trajectories of individual particles as a result of a force balance taken on each particle (see Equation 4). By assuming different initial locations and sizes and using statistical techniques, we can calculate the motion of the particle phase and its interactions with the fluid. In the Eulerian approach, conservation equations embodying postulated constitutive relations are solved to predict the field distributions of momentum and volume fraction of each phase. The form of the Eulerian particle momentum equation is closely connected to its Lagrangian equivalent, because the former can be derived from the latter by averaging over the particle phase. In both the approaches, the particle–fluid momentum equations are coupled through the drag source/sink terms and through the volume fraction of the particle phase. If the volume fraction of particles is very small, two-way coupling between the phases is reduced to the drag interactions mutually induced. A one-way coupling condition exists when the influence of particle drag on the momentum balance of the fluid phase is negligible.

The relative advantages and disadvantages of Lagrangian and Eulerian descriptions of particle motion have been argued.[122–125] Because the Lagrangian approach yields a more detailed physical description of the particle phase (such as individual particle speeds, trajectories, and residence times), it is more germane than the Eulerian description to the problem of predicting erosion. The Lagrangian approach appears to be less prone to numerical diffusion errors, is more stable for flows with large particle velocity gradients, and is readily applied to

polydispersed particle systems. On the negative side, in concentrated systems with significant particle–fluid and particle–particle interactions: (a) model formulations are inadequate owing to a lack of fundamental understanding concerning the interactions; and (b) limitations related to computer storage, calculation times, and convergence exist.

In principle, the Eulerian description is favored by high concentrations of the particle phase. Through rigorous definitions of averaging procedures, it offers a formal methodology for developing numerical models dealing with direct and indirect particle interactions and fluid turbulence.[100,126–129] Despite its formal framework, however, in practice the continuum modeling of interactions leading to constitutive relations for particle–particle and particle–fluid stresses is in its infancy. The reason is the same as for the Lagrangian approach: an insufficient understanding of the complex particle–particle and particle–fluid interactions that develop in turbulent flow and the mathematical complexities of representing these phenomena, even as averages. However, we cannot deny the usefulness of formal Eulerian formulations, and the potential of hybrid Lagrangian–Eulerian formulations is yet to be explored. In a hybrid approach to predicting erosion, for example, the particle phase could be described by a Lagrangian formulation near surfaces and by an Eulerian formulation away from surfaces.

For the Eulerian description of particle–fluid motion the question arises: Under what conditions can the dispersed particle phase be viewed as a continuum? The question is important because, in principle, the continuum framework greatly facilitates the derivation of formal theoretical relations describing the influence of particle–fluid and particle–particle interactions in the mixture flow, which can be of great computational advantage. In formulating a set of averaged field equations appropriate to fluid–particle flows, postulating macroscopic equations without reference to microscopic details may be preferable.[130,131] But, for guidance, we should consider Drew's averaging methods[100,126,127]—and those of others—and look to the discrepancies between measurements and predictions of relevant flow variables to assist in the convergence of this approach.

The continuum equations proposed by Hinze[93,130] have been the basis for Eulerian calculations of particle-laden turbulent flows. The equations are obtained by applying the Reynolds decomposition procedure, followed by averaging the instantaneous transport equations. Extended forms of these equations and the constitutive relations have been used for calculating erosive wear in curved channels,[82] to calculate particle dispersion in a mixing-layer flow,[118] and to predict solid–liquid suspensions in stirred vessels.[132] Even if the particle phase is dilute ($\alpha \ll 1$), there must be a sufficient number of particles in the smallest turbulent eddy to appropriately define statistical averages of particle-related variables, such as density and velocity. Hinze,[93] addressed this point and suggested that $s/\eta \leq 0.1$, where s is the average separation distance between particles, for the concept of a continuum to apply. However, Hinze gives examples of continuum formulations that proved applicable in situations that did not meet this criterion.

3.2.5 *Numerical modeling and applications.* Among the major contributions to the subject of predicting particle motions in systems of engineering interest is the classical analysis performed by Taylor[133] for raindrop impingement and icing on aircraft wings. In that study, he pursued a Lagrangian formulation in which the force acting on a particle was attributed solely to mean flow drag. Taylor considered both Stokes' and Newton's resistance laws for specifying the particle drag coefficient. However, he focused on solutions for the former condition only, for the cases of inviscid stagnation point flows on a flat surface and on a large cylinder, respectively. Taylor found that, for values of the particle inertia number $\lambda < \frac{1}{4}$, if at any time a particle is traveling at fluid velocity, at no subsequent time will it strike the surface. For $\lambda > \frac{1}{4}$ a particle always strikes the surface, provided that at some time in its trajectory it moves at fluid velocity.

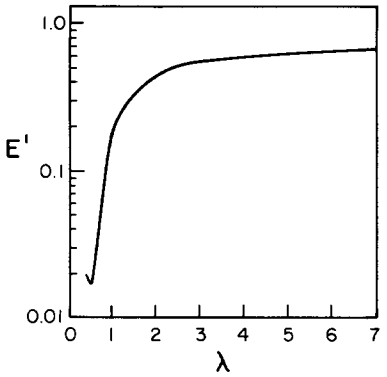

Figure 5 Effect of particle momentum equilibration number, λ, on the relative erosion of a wall in a region of 2-D stagnation point flow. In the figure, $E' = E \times$ total mass of particles striking the surface. $E' \propto V_1^3$ for $n = 2$ in Equation 1. The steep rise in erosion is caused by the strong dependence of V_1 on λ. Based on calculations by Laitone[37]

From his analysis, Taylor drew various important qualitative conclusions pertaining to the density distribution of surface-particle impacts. In later studies of the same problem and using Taylor's analytical approach, Laitone[35,37] quantified the surface–particle flux distribution as well as particle impact angles and speeds, as functions of initial location, initial velocity, and inertia number. Hethen calculated erosion using these results in conjunction with an empirically adjusted cutting wear model.[8] The relative rate of erosion predicted by Laitone[37] is shown in Figure 5 as a function of the particle inertia number, λ. The rate of erosion increases by more than one order of magnitude when λ goes from 0.4 to 2. The minimum shown in the erosion curve, between $\lambda = 0.25$ and 0.4, results from the reduced particle impact velocity in this range of λ. From the analytical model, Laitone established a range for the variation of the exponent in the velocity dependence of erosion (see Equation 3). As discussed in the Introduction, the range predicted for the exponent is in agreement with experimental findings and, more important, the analysis affords a purely fluid mechanics interpretation of the exponent variation in velocity, as opposed to a materials-related interpretation.

In their studies, Taylor and Laitone assumed inviscid flows in determining fluid velocity. (Viscosity entered the formulations only as a way to determine the drag force acting on a particle because of a resistance law.) Such an approach yields no information on possible boundary-layer effects on particle motion and erosion. Near a solid surface the no-slip condition imposes a surface-normal gradient in the fluid velocity component tangential to the surface. This gradient, in turn, can affect the drag exchanges between fluid and particles traversing the boundary layer. Wenglarz investigated the problem analytically for turbulent flow, by prescribing a $\frac{1}{7}$ power-law distribution for the mean tangential velocity component of the fluid phase.[134] He used this velocity distribution as the driving force in the tangential component of the Lagrangian particle equation of motion to calculate the effects of a boundary layer on the impact speeds and incidence angles of particles entering the boundary layer with specified initial velocity components.

These studies illustrate the value of analytical approaches for investigating particle motion and erosion in relatively simple flow configurations with one-way (fluid-to-particle) coupling.

Other examples are References 90, 135, and 136. However, most flows of engineering interest are three-dimensional (3-D), turbulent, and often constrained by highly complex boundary conditions. For such systems theoretical analysis must be performed numerically, using high-speed, large-storage computers.

Numerical calculation approaches for particle-laden flows can be divided into two groups, according to whether the particle phase is considered discrete or continuous. Further subclassification follows, according to whether the particle phase is dilute or concentrated and one-way or two-way coupling considerations apply and whether the flow is laminar or turbulent. For turbulent flows, final classification depends on the closure method (turbulence model) used. Examples of numerical procedures developed and applied to predict erosive turbulent flows include Lagrangian (discrete particle phase) formulations[38,39,83,137] and Eulerian (continuum particle flow) formulations.[82] My colleagues and I at Berkeley used a deterministic two-equation k–ε model of turbulence to simulate the turbulence of the fluid phase. Even though limited by the assumption of an isotropic turbulent viscosity, this model illustrates the importance of turbulence in particle dispersion and erosion. In principle, more accurate simulations of the anisotropic erosive flows typical of the industry should be possible with more advanced closure methods,[79,80,138,139] but these approaches can be computationally intensive, especially for 3-D configurations. Most investigators simply take the mean motion of the fluid field to act as the driving force in the particle equation of motion. However, studies in which velocity fluctuations have been directly superimposed on the mean flow[83,103,107,113,114] show that the resulting *turbulence drift velocity* of the particle phase can be significant.

In the remainder of this section, we briefly review a few examples of Lagrangian model formulations used to predict particle motion and erosion in some complex flows of engineering interest.

Turbomachinery flows. Two-phase flows through turbomachinery equipment and related system components are of considerable importance to the power and transportation industries. Gas turbines in ground vehicles, aircraft, and naval installations are frequently operated in highly erosive, particle-laden environments containing sand, dust, or salt.[21] Many of the power plants being considered for utilization of coal-derived fuels will have to contend with the presence of particles in the expansion gases flowing through the combustion turbines. For them, determining the level of gas cleanup that will allow an acceptable, safe, and reliable turbine performance is imperative.[140] Erosion in steam turbines can be caused by water droplets or scale displaced from the inner surfaces of steam-generator tubes. Units that frequently undergo start-up and shutdown encourage scale displacement, and blade replacement is necessary after about 40,000 hours to avoid secondary damage to the turbine.[141] Numerous studies and references on problems caused by liquid-impact turbine erosion are available in the proceedings of the International Conferences on Erosion by Liquid and Solid Impact held periodically in Cambridge, England.[142,143] Although we do not discuss erosion by liquid-droplet impact here, much of what we say about calculating solid-particle trajectories in turbomachinery flows applies.

Early theoretical studies on the degradation of turbine performance by particles lagging behind the gas phase—both in velocity and temperature—suggested the importance of erosion. It can change blade shape, which degrades turbine performance and ultimately leads to blade failure.[144–146] As a result, numerical methods were developed for calculating solid-particle trajectories in axial flow compressors and turbine stages that model the particle impacts with the blades and their subsequent rebounds.[147–149] The blade airfoil shape and the blade-to-blade flow field at the mean radius were included in the 3-D particle trajectory calculations.[147,148] The only force considered in the particle equation of motion was that caused by fluid drag. Lines of best fit applied to experimental data were used to predict the magnitude and direction of particles rebounding from the blade surfaces.

Grant and Tabakoff subsequently modeled the heterogeneous nature of particle flows through turbomachinery using a Monte Carlo method to simulate particle ingestion and subsequent erosion.[149] They chose specific conditions for individual particles at random from prescribed statistical distributions of particle size, particle location, rotor location, and the restitution ratio. Using deterministic equations, they calculated the motion of the particle and by considering a large number of particles, obtained the statistical solution to the heterogeneous particle flow and erosion problem.

Applications of these numerical procedures have been restricted to inviscid flows in two-dimensional (2-D) blade-to-blade channels, based on the assumption of zero radial gradients in either the flow configuration or its properties. Therefore the procedures used are not suited for particle trajectory calculations of inlet flow fields. These fields are characterized by significant hub and tip contouring, and the 2-D approach cannot represent the variation of the flow field and vane shape in the radial direction. Hamed[150] removed these limitations by using Katsansis and McNally's 3-D, inviscid, numerical calulation procedure.[151] In this procedure the flow field solution is obtained on a mid-channel, hub-tip stream surface using a finite difference stream-function formulation for subsonic flow and a blade-to-blade velocity gradient method for transonic flow. Improved applications of this approach for predicting erosion patterns produced by particles rebounding from twisted blades have been reported.[152,153]

Other calculations of particle trajectories and erosion based on inviscid, 3-D solutions of the fluid-flow field have been performed along the lines of the studies discussed previously.[137,154–156] Figure 6 illustrates the type of particle trajectory predictions from which Menguturk and Sverdrup[137] were able to make specific recommendations for cleaning turbine expansion gas. This work involved a detailed parametric investigation of the flow and erosion by coal-gas ash particles in the first stage of a large electric utility gas turbine. It was based on projected particle distributions in the gas leaving the cleaning system of a pressurized fluidized-bed gasifier system. Some of the problems related to scaling experiments in cascades and small turbines—to simulate particle and erosion through large utility turbines in advanced coal-fired power plants—are discussed in Reference 154. Although difficult to perform, such experiments are essential for determining gas cleaning requirements for successful turbine operation. To avoid the experimental problems, Wenglarz and Menguturk evaluated numerically the relative effects of physical scale, rotation speed, and pressure differences on erosion, using the erosion damage model of Reference 137. Using a simplified version of the same procedure, Wenglarz performed a numerical exploration of the erosion potential throughout the expansion section of a multi-stage turbomachine.[155] Gunes and Menguturk[156] showed the importance of accurately resolving the flow field near the blade leading edge in order not to invalidate subsequent particle trajectory calculations in gas turbine blade passages.

These and similar inviscid flow numerical investigations complement what have always been very difficult experiments to perform. In general, broad qualitative agreement has been found between predicted patterns and rates of erosion of exposed turbomachinery surfaces and the limited experimental data available. This agreement has further encouraged the use of numerical work for predictive purposes, resulting in a wealth

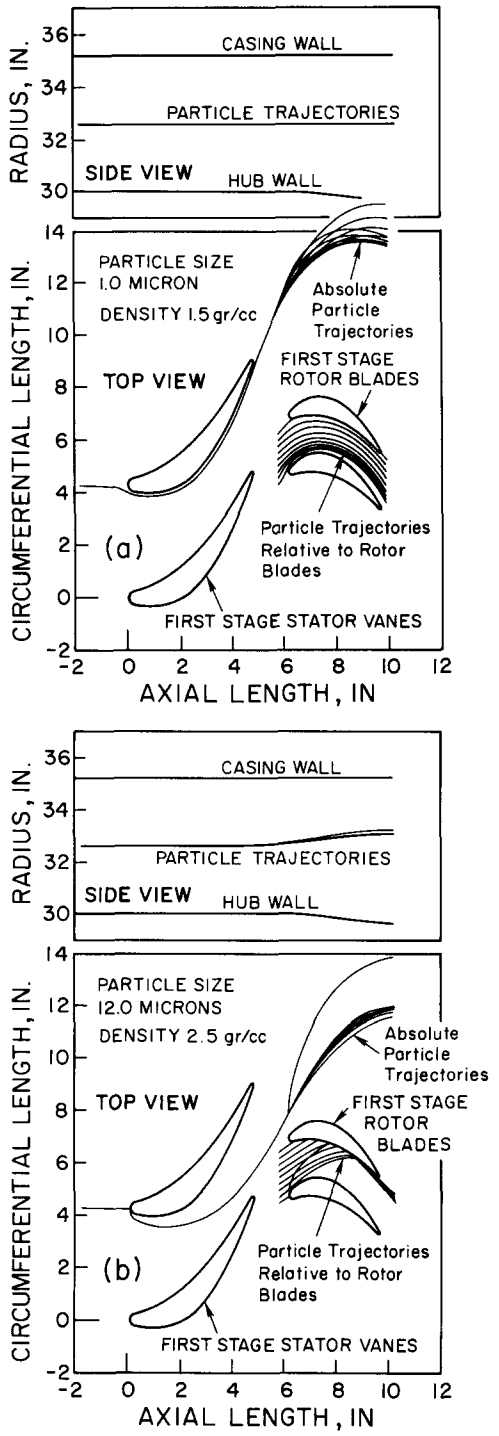

Figure 6 (a) Trajectories of 1-μm ash particles and (b) 12-μm dolomite particles passing through the stator and rotor passages of a turbine. The top portions show the trajectories in the flow channel. The bottom portions are the top views of the axisymmetric blade-to-blade stream surfaces. Because of their inertia, the large particles collide several times with the first-stage rotor blade. Based on calculations by Menguturk and Sverdrup[137]

of information for which there often is no experimental counterpart. For example, the trajectories of the large particles shown in Figure 6 are dominated by impact–rebound phenomena, the large relaxation times being responsible for the reduced influence of the flow field on their trajectory. Small particles with $\lambda < 1$ rapidly acquire the local gas velocity after each impact, with the possibility that subsequent impacts increase erosion damage. Near swirling vanes, large particles striking a hub can reenter the engine core's flow field after hitting the tip. This action reduces separator effectiveness and increases erosion of later turbine stages. Maximum erosion from large particles occurs at the blade hub near the trailing edge. As particle size decreases, the location of maximum erosion on the blade moves both radially and axially away from the hub's trailing-edge corner.

Cascade and small turbine experiments do not yield erosion rates and erosion tolerances typical of large utility turbines. Therefore measurements of simulated erosion rates can differ from utility erosion rates by up to an order of magnitude. The effects of physical scale, rotation speed, and pressure differences must be considered carefully in attempts to apply experimental and numerical results obtained in simulation devices of large utility turbines. Velocity triangle variations and progressive gas expansion contribute significantly to the differences in erosion between stages in multistage turbomachines. Gas expansion results in reduced particle concentration and hence reduced flux to blade surfaces, tending to decrease erosion progressively through the turbine's stages. However, the effect is somewhat offset by reduced drag forces acting on the particles, which, in deviating from the fluid streamlines, can strike the blade surfaces with more adverse impact angles.

Boundary layers and secondary flows. While inviscid flow methods have been used widely in turbomachinery applications, more generally applicable viscous flow procedures are gaining popularity in these and other complex configurations.[79,157–162] Boundary layers and secondary cross-stream flows are characterized by strong viscous effects that can alter the relative velocities, and hence the potential for erosion, of particles moving near or toward surfaces. For example, a high-speed particle penetrating a lower speed boundary layer will decelerate. Depending on the new incidence angle, the slower moving particle may have less erosion potential.

A major factor in determining the magnitude and extent of boundary-layer-reduced erosion is the particle inertia number, λ. If, in the definition of λ (see Section 3.2.1), we substitute for the characteristic length the boundary layer thickness, δ, and for the mean velocity of the fluid phase the component of particle velocity normal to the surface, V_N, evaluated at $y=\delta$, we get

$$\beta \equiv \frac{\delta}{s} = \frac{\delta}{V_N d_p^2 \rho_P / 18\mu} \tag{13}$$

The quantity s in Equation 13 is referred to as the particle *stopping distance*. It is a conservative estimate of the maximum distance a particle is expected to travel at constant mean speed V_N in the direction normal to the surface—starting at the edge of the boundary layer along that surface—before it adjusts to the local mean velocity, which (within the boundary layer) is primarily aligned parallel to the surface.[134] Only for values of $\beta < 1$ will particles penetrate a boundary layer deeply enough to strike and possibly erode a surface.

Menguturk *et al.* modeled numerically the effects of a boundary layer on particle deposition and erosion for conditions typical of turbine flows by matching an inviscid outer-flow solution to a 2-D compressible boundary-layer flow calculation.[163,164] The lack of experimental information forced them to assume a unit-particle deposition ("sticking") probability. They predicted erosion rates using the model of Reference 137. Based on their numerical results, we can distinguish among three main regimes for particle transport within a boundary layer: (1) a Brownian or molecular diffusion regime ($d_p \leq 0.1$ μm), characterized by very small particles transported mainly by

molecular diffusion; (2) a turbulent diffusion regime ($0.1\,\mu m \leq d_p \leq 1\,\mu m$), characterized by the transport of particles that diffuse under the influence of turbulent fluctuations; and (3) an inertial regime ($d_p > 1\,\mu m$), characterized by particles moving under the influence of their own inertia.

These numerical studies[163,164] were conducted for specific turbine stages, and the results do not lend themselves readily to general interpretation. However, calculations in the inertial regime agree well with the more general analysis in Reference 134. Although the numerical results strongly suggest that boundary-layer induced particle deposition can seriously degrade the performance of a turbine stage, the calculations are subject to serious uncertainties owing to the lack of accurate information concerning particle deposition probability.

In relation to erosion, viscous flow analysis[134] shows that: (1) the presence of a boundary layer always decreases particle impact speed and increases particle impact angle (relative to the normal to the surface); (2) these two effects are significant only for boundary layers containing particles with $\beta > 0.4$ but can substantially reduce erosion; (3) because of the characteristic erosion incidence-angle dependence of ductile materials, the erosion of ductile surfaces impacted by particles with $\beta < 0.4$ can also be markedly reduced over a narrow range of particle boundary-layer entry angles; and (4) in an application of the theory to rotor trailing-edge erosion, for flow conditions typical of large turbines, significant boundary-layer-reduced erosion occurred only for particles of less than about 4 μm in diameter.

Secondary motions arising from lateral curvature of the main flow can significantly affect the velocity and erosion potential of small particles. Mason and Smith[165] clearly demonstrated this effect in various curved flow configurations. They performed experiments in curved duct sections made from transparent plexiglass in order to visualize the time-dependent effects of primary and secondary motions on erosion. Turbulent air flows of dilute ($\alpha \simeq 10^{-3}$) suspensions of alumina particles ranging from 50 to 60 μm in diameter were passed through two 90° bends of square cross section of bend curvature to radius ratios of $2Rc/D = 20$ and 12, respectively. The duct flow Reynolds number varied between $Re_D = 88{,}000$ and 152,000, approximately, and the mass loading ranged from $\gamma = 0.5$ to 3.8 kg alumina/kg air. Mason and Smith first observed erosion at a bend angle of 21° on the concave surface, where a wear "pocket" gradually formed. After the pocket attained a critical depth, erosion became noticeable on the convex surface of the bend between 30° and 60°, approximately, the extent and amount of wear depending on flow speed and particle concentration. The change in surface shape at the convex wall produced further changes in the secondary flow patterns through the bend, leading to the formation of secondary and tertiary wear locations on the concave wall, at 70° and 87° bend angles, approximately.

These experiments clearly showed that secondary motions can significantly influence erosion and that the secondary motions themselves are subject to change as surface topography is reshaped by the erosion process. However, numerical simulations of these flows, based on a continuum formulation for the particle phase and *neglecting* the secondary motion (i.e., assuming a curved channel), have yielded erosion results along the concave wall in broad qualitative agreement with the measurements.[82] Figure 7 compares these results, showing that the discrepancies increase with increasing Reynolds number because of the more pronounced effect of the secondary flow on particle motion. Other numerical evaluations of the effect of secondary motion on erosion in curved passages are presented in References 166–169.

Impinging jets and cylinders in cross flow. Particle-laden jets impinging on surfaces are used extensively in erosion experiments to investigate resistance of materials to wear, usually under accelerated erosion conditions.[6,170–172] High-pressure water jets containing abrasive particles are used to cut advanced materials in numerous industries.[173] Cases of cylinders in cross flows with eroding particles occur in heat exchange equipment, including the convective zone (freeboard) of a fluidized-bed combustor, and in the primary superheaters, reheaters, and economizers of coal-fired boilers.[174]

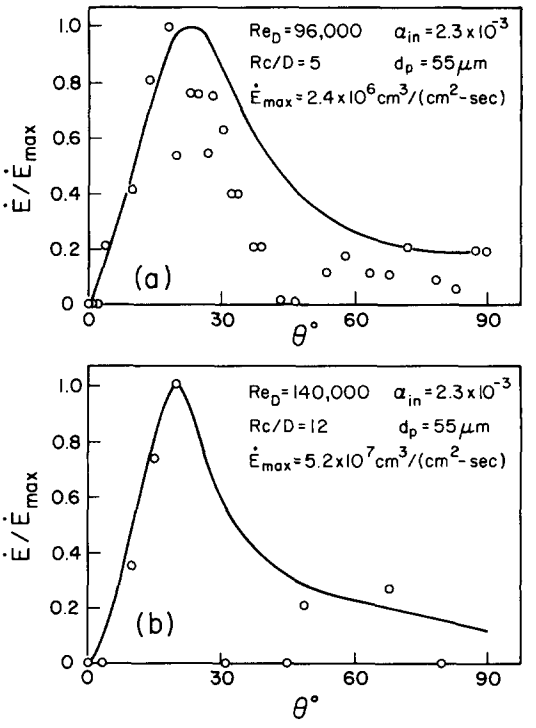

Figure 7 Two-dimensional prediction of the rate of erosion at the concave wall of a 3-D curved duct flow; θ is the bend angle along the channel. (a) Strong curvature and (b) mild curvature. Based on measurements (dots) by Mason and Smith[165] and calculations (lines) by Pourahmadi and Humphrey[82]

Taylor[133] performed the first detailed analysis of particle-laden impinging jet flows. Subsequently, Laitone[35,37,38] investigated this configuration, as well as the case of particle-laden flows past cylinders. (We discussed these seminal studies in Section 3.2.5.) The main point here is the complete absence of turbulent flow considerations in these and similar erosion analyses. My coworkers and I at Berkeley have tried to redress this deficiency. Two of our contributions are briefly reviewed.

The influence of turbulence on erosion by spherical sandlike particles suspended in an air jet impinging normal to a flat solid surface was first investigated by Dosanjh and Humphrey.[39] Using a two-equation (k–ε) turbulence model, we calculated the mean motion of the fluid which we then used as the driving force in the deterministic Lagrangian equation of motion applied to each particle. Thus we evaluated the effect of the turbulence on the particles *indirectly*, through its effect on the mean motion of the fluid. We predicted impacting particle speeds, incidence angles, and particle surface densities from the particle equation of motion. We subsequently calculated erosion from these data, using a cutting wear model for ductile metals.[6] This work represented a numerical attempt to establish the qualitative dependence of surface erosion on fluid jet turbulence intensity, as this type of experimental data is unavailable. The particular metal surface–particle pair chosen for investigation[39] is immaterial, because the erosion predictions can be presented in nondimensional form. Figure 8[39] shows the influence on

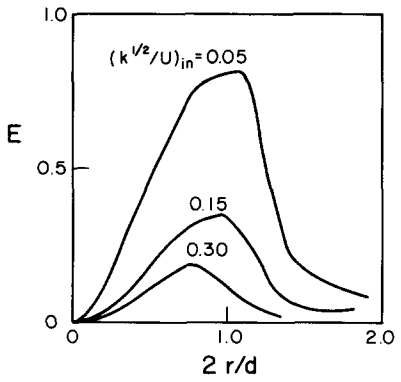

Figure 8 Erosion by a dilute particle-laden gas jet striking a flat surface perpendicularly; r is the radial coordinate along the surface from the stagnation point, d, is the jet nozzle diameter, k is the turbulent kinetic energy of the gas flow, and U is the mean jet velocity. The values of k and U are specified at the jet origin. Based on calculations by Dosanjh and Humphrey[39]

erosion from altering the level of turbulence imposed in the air jet. Erosion decreases with increasing turbulence intensity. Although perhaps counterintuitive, this finding is partly explained by the fact that both particle impact speed and particle flux to the surface decrease with increasing turbulence. Both effects are related to the increased radial dispersion of particles and lead to diminished erosion, as predicted by the cutting wear model.

The results in Figure 8 also show that the position of maximum erosion is significantly displaced toward the jet-symmetry axis with increasing turbulence intensity. The reason is that, according to the cutting wear model, maximum wear occurs for particle incidence angles of about 25° with respect to the surface, and the effect of increasing turbulence intensity is to alter (in the way shown) the position on the surface where this angle is attained.

Although limited by the simplifications made in the analysis, our findings[39] showed that fluid turbulence can significantly alter particle impact and thus erosion and that computational fluid dynamics procedures can be usefully applied to flow configurations of engineering interest. In such a procedure, the mathematical detail with which the fluid and particle equations of motion must be formulated to accurately represent the flows—and the extent to which the two phases must be coupled in a formulation—are very problem specific. For many practical configurations involving erosion by dilute particle-laden gases, one-way coupling, within the context of a phenomenological closure method such as the k–ε model referred to, may be sufficient to correctly establish significant effects. This result is further illustrated by reference to the erosion of cylinders in cross flow, discussed next.

Our ideas were subsequently extended by Schuh *et al.*[83] for the case of an initially turbulent particle-laden air stream flowing past one or two in-line tubes or past a tube in an in-line tube bank. We used a nonorthogonal, body-fitted calculation approach to represent the tube configurations investigated. As in the jet case, one-way coupling was assumed and the fluid turbulence was described by means of the two-equation k–ε model, with a logarithmic relation to describe the velocity on either side of the boundary-layer separation point on a tube. The effect of the turbulence on particle motion was modeled two different ways: either deterministically[39] or stochastically,[103] by superposing a random distribution of turbulent fluctuations on the calculated mean fluid flow and using it as the forcing function in the particle equation of motion. In the latter case, tracking a statistically significant number of particles released at different locations in the calculation domain allowed calculation of average particle quantities and erosion. Figure 9(a) and (b) show calculated deterministic and stochastic particle trajectories for the case of two in-line tubes for identical problem conditions.[83] Note that, unlike the stochastic calculations, the deterministic results for the particles with low inertia number ($\lambda < 0.1$) do not show these particles striking the second downstream cylinder. However, the associated erosion was negligible.

Among other things, the results reported in Reference 83 illustrate the importance of accounting more realistically for the influence of fluid turbulence on particle motion in erosive flows. With the availability of greater computing power, more accurate finite differencing methods, and more sophisticated numerical algorithms, we can increasingly expect to see phenomenological modeling approaches being complemented by direct numerical simulation techniques capable of more accurate (model-free) representations of particle-laden turbulent flows.[175,176]

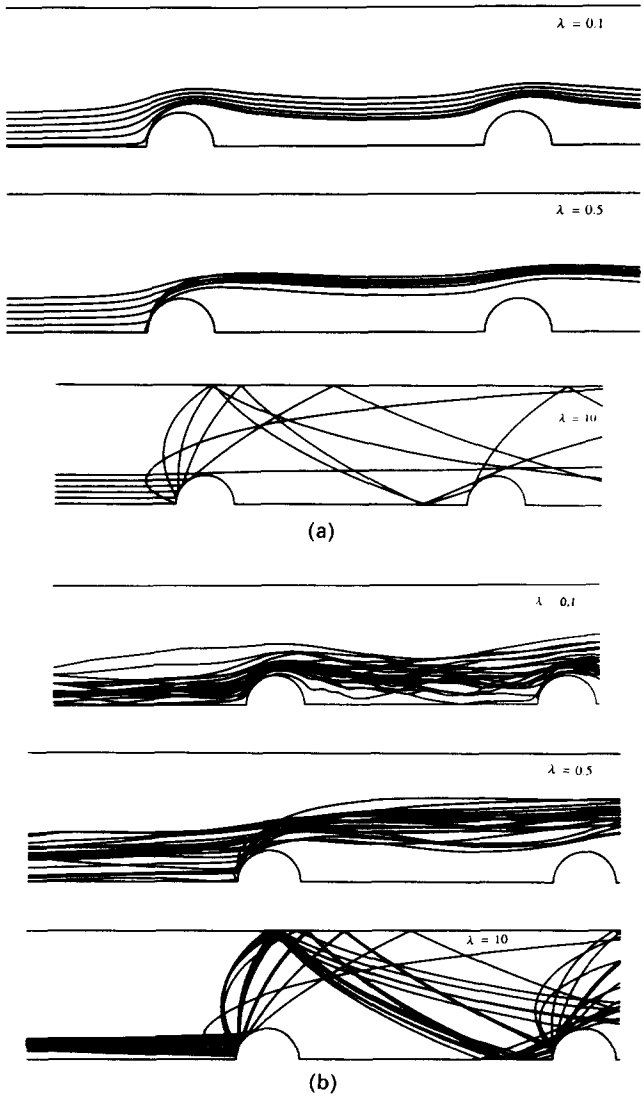

Figure 9 (a) Deterministic and (b) stochastic predictions of particle trajectories for the flow past two in-line tubes. Three momentum equilibration numbers considered for a flow with Reynolds number (based on tube diameter) $Re_D = 2.94 \times 10^4$. Based on calculations by Schuh *et al.*[83]

3.3 *Particle–surface interactions and related phenomena*

3.3.1 *Determining restitution coefficients.* The experimental measurement of particle restitution coefficients is difficult,[73,148,149,177–179] but the information is necessary for solving the equations governing the trajectories of particles rebounding from surfaces and subsequently striking the surface again. The data are generally provided as least square fits to polynomial functions of the form:

$$\frac{V_2}{V_1} = a + b\beta_1 + c\beta_1^2 + \cdots$$
$$\frac{\beta_2}{\beta_1} = a' + b'\beta_1 + c'\beta_1^2 + \cdots \quad (14)$$

where V_1 and β_1 are the particle incidence speed and angle and V_2 and β_2 the corresponding rebound values, with β_1 and β_2 measured relative to the tangent to the surface, at the impact location, in the V_1–V_2 plane. The numerical values of the coefficients a, b, c, etc., in Equation 14 depend on the material properties of the specific particle–surface pair. Similar data for the *rotation* velocities of particles rebounding from surfaces apparently are unavailable.

Armstrong *et al.*[179] designed an apparatus in which the fluid medium was essentially stagnant around the target surface material, at which high-speed particles were aimed. This apparatus allowed them to separate particle impingement phenomena from fluid flow effects, permitting investigation of the influence of the Magnus force on particle trajectories. More realistic conditions involve large spatial and temporal variations of fluid flow conditions in the vicinity of the target.[73,148,149] However, such conditions are considerably more difficult to control and measure, because they require the use of nonintrusive techniques, especially close to the impacted surface.

The restitution characteristics of particles rebounding from surfaces require a statistical description. For fixed incidence values β_1 and V_1, the rebound values β_2 and V_2 have statistical distributions resulting from (a) variations in particle shape, size, and rotational velocity at the time of impact; (b) variations in the topography and properties of the test surface; (c) uncontrollable phenomena, such as particle and/or surface fragmentation, particle–particle collisions, changes in properties of materials owing to sudden highly localized temperature increases; and (d) variations in near-surface fluid flow conditions, which significantly affect particle trajectories if $\lambda < 1$. In addition, measurement uncertainties are associated with the experimental techniques, which must remain small if meaningful results are to be obtained.

Figure 10 is a histogram showing a typical statistical distribution of the velocity restitution ratio for the case of relatively hard particles striking a ductile surface. Measurements such as these show that the shapes of the distributions for V_2/V_1 and β_2/β_1, as well as the mean values of these ratios, vary strongly with β_1. Nevertheless, all attempts to date to use restitution coefficient information at boundaries for predicting particle trajectories and erosion have been limited to the use of the mean values of the distributions, with the information contained in the *shape* of the distribution being ignored. This practice raises serious questions about the validity of predictions of particle trajectories and surface wear locations when the particles are subjected to sequential impacts, such as in turbomachinery.

The distributions of V_2/V_1 and β_2/β_1, as well as their variations with the incidence angle, β_1, are highly dependent on the physical properties of the impacting particle/impacted material surface pair. For example, all the polymeric materials tested by Brauer,[177] using 6-mm diameter steel spheres in free fall, gave rebound angles larger than incidence angles for all values of the incidence angle tested. By contrast, most of the metals gave rebound angles smaller than the incidence angles. The data reported in Reference 73, for much smaller particles in much faster flows, show that for small incidence angles, β_1, the ratio β_2/β_1 is greater than 1 and that as β_1 increases, β_2/β_1 becomes substantially less than 1. The highly specific dependence of the restitution coefficients on the materials involved, and the unknown influence of transverse Magnus and Saffman forces, make deriving general theoretical relations or postulating generally applicable empirical correlations for these from the experimental measurements very difficult.

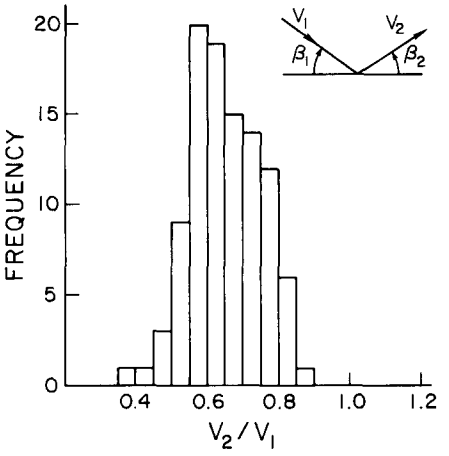

Figure 10 Histogram for the velocity restitution ratio V_2/V_1 corresponding to 200-μm quartz particles striking 410 stainless steel at $V_1 = 76.2\,\mathrm{m\,s^{-1}}$ with angle $\beta_1 = 15°$. Histogram based on 101 observations. Based on measurements by Tabakoff and Sugiyama[73]

3.3.2 *Particle fragmentation and multiple impacts.* Particle fragmentation and secondary erosion have been discussed in various works.[17,18,46,180,181] Experiments show that under certain conditions particles shatter into smaller fragments upon striking a surface. The fragments move radially outward, their circumferential distribution depending on the impact angle, causing what has been called by Tilly and Sage[19] *secondary erosion.* They concluded from their observations that the fragmentation process, especially the resulting fragment sizes and speeds, depends on the physical properties of the pair of particle and surface materials involved and on initial particle size and speed. Apparently, each pair of materials has a threshold size below which fragmentation does not occur. Some materials also have a saturation level, beyond which fragmentation becomes independent of particle size.

Uuemois and Kleis[20] analyzed the effect of particle fragmentation on erosion. They pointed out that the velocity exponent, n, in the expression for erosion given by Equation 1 can either increase or decrease at a critical impact velocity that depends on the pair of materials involved. Cases in which n increases involve the erosion of soft and ductile materials by abrasives that are damaged only slightly upon impact. Cases in which n decreases, at a definite critical velocity, are generally observed when hard and brittle abrasives strike even harder surfaces. The critical velocity threshold marks the beginning of particle disintegration. Even though the resulting fragments acquire high speeds and are capable of significant secondary erosion, they form at the expense of the parent particle's kinetic energy. Uuemois and Kleis estimated[20] that a 1% loss of initial particle mass, in the form of radially ejected fragments, can reduce the normal component of kinetic energy of the impacting parent particle by 16%. If secondary erosion is less than the

erosion that would be caused by the unfragmented particle, the velocity exponent n should decrease.

In principle, particle fragmentation should help to reduce the total amount of erosion, but the overall picture is complicated by the poorly understood influence of turbulent fluctuations and particle–particle interactions on particle motion. As a result, the smaller fragments may well be the cause of additional, often critical, erosion at previously unworn locations through repeated or multiple impacts.

Although he did not address particle fragmentation in a study on the effects of multiple impacts, Laitone[38] predicted the trajectories of nonspinning particles rebounding from cylindrically shaped surfaces for flow conditions typical of jet turbines. He restricted his attention to dilute systems composed of sandlike particles in air, for which the dominant force acting on the particles was caused by the fluid-induced viscous drag. He adapted Chorin's vortex scheme[182] to predict the high-speed, unsteady, recirculating viscous flow past a cylinder. This method is entirely Lagrangian and simultaneously tracks both fluid vorticity (as discrete vortex "blobs") and particles (as coagulated packets). Laitone used experimentally determined average restitution parameters to specify normal and tangential particle component velocities after impaction with the cylinder. Typical results for repeated particle impacts are shown in Figure 11. These calculations reveal that particles with $\lambda = 1$ in a flow with $\mathrm{Re} = 10^5$ can experience substantial acceleration between the first rebound and their second impact with a cylinder. The observation is significant for erosion, because it means that a large fraction of the original kinetic energy may be restored to a particle accelerating around a blunt object between a primary and a secondary impact. Although subject to large uncertainties —and highly specific to the case of 200-μm quartz particles striking 2024 aluminum alloy—the rebound correlations allowed Laitone to conduct a qualitative assessment of the frequency of multiple particle impacts and the attendant "secondary" erosion.

Laitone's calculations also show that, near the stagnation point on the cylinder, potential flow theory and viscous calculation methods yield essentially identical particle trajectories. Overall, however, the inviscid approach tends to overestimate wear because of the absence of a boundary layer, which slows

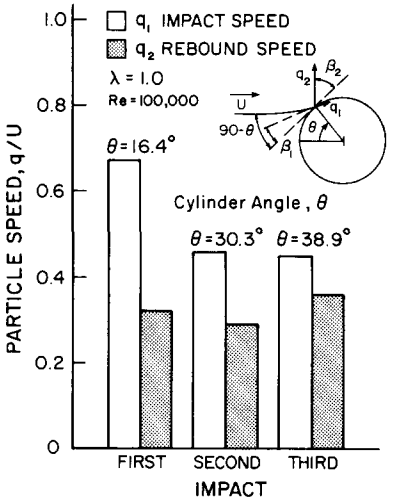

Figure 11 Variation of particle velocity with impact location θ for a triple impact and rebound with a cylinder surface. The difference in impact and rebound speeds is proportional to the momentum lost by the particle in performing erosive work on the surface. Secondary erosion from subsequent impacts is nearly 50% of primary erosion from first impact. Based on calculations by Laitone[38]

down and helps to deflect particles around blunt objects. The effect of viscosity becomes pronounced beyond a cylinder angle (measured from the stagnation point) of 10°. The trajectories of particles with inertia numbers $\lambda < 1$ were strongly affected by eddy shedding from the cylinder, resulting in particle entrainment and crossing trajectories in the wake-flow region. Experimental evidence supporting these findings is reported in Reference 183.

3.3.3 *Magnus and Saffman forces.* In addition to the viscous drag force, $\vec{F}_D$, experienced by a particle that is in relative motion with respect to the fluid around it, two forces that act orthogonally to the particle's direction of motion can develop and significantly affect its erosion potential. One, caused by particle rotation, is referred to as the Magnus force.[184] The other, resulting from fluid shear, is the Saffman force.[185] Both are the result of inertia effects in the flow field around the particle and have been studied extensively for the case of spheres, to which we limit the discussion here.

A theoretical derivation of the Magnus force for the case of $\mathrm{Re}_p \ll 1$ was performed by Rubinow and Keller,[184] who found that

$$\vec{F}_M = \pi \rho_f \left(\frac{d_p}{2}\right)^3 \vec{\Omega}_p \times \vec{U}_p \tag{15}$$

This expression states that a spherical particle with angular velocity $\vec{\Omega}_p$ moving at mean velocity $\vec{U}_p$ in a viscous fluid at rest experiences a force $\vec{F}_M$, transverse to the particle's direction of motion and with the sense indicated by the vector product. This result is independent of the fluid viscosity.

Saffman[185] showed that, if the motion of the particle takes place relative to an unbounded fluid in uniform viscous shear, a transverse force will act on the particle:

$$\vec{F}_S = k_s \rho_f \left(\frac{d_p}{2}\right)^2 \left[\frac{\nu}{|\vec{\Omega}_f|}\right]^{1/2} [\vec{\Omega}_f \times (\vec{U}_p - \vec{U}_f)] \tag{16}$$

where $k_s = 6.46$ is a constant and $\vec{\Omega}_f$ is the fluid vorticity. To order $O(\nu^{-1/2})$, this result is independent of particle rotation and is strictly valid only when the particle's translational, shear, and rotational Reynolds numbers, respectively, are $\mathrm{Re}_p \ll 1$, $\mathrm{Re}_s \ll 1$ and $\mathrm{Re}_r \ll 1$, with $\mathrm{Re}_p^2/\mathrm{Re}_s \ll 1$. These restrictions limit the applicability of Equation 16 to small particles that are almost neutrally dense with respect to a low-speed fluid that transports them. The particle translational and shear Reynolds numbers are as defined earlier. The rotational Reynolds number is defined as $\mathrm{Re}_r = d_p^2 \Omega_p / \nu$, where Ω_p is the modulus of the particle's angular velocity, $\vec{\Omega}_p$.

Equations 15 and 16 have provided the basis for successful numerical simulations of various qualitative features concerning the radial migration of particles in liquids in pipe flow.[186] However, in many engineering devices involving solid particulates suspended in high-speed gas streams, the Reynolds number constraints (particularly $\mathrm{Re}_p \ll 1$) are not met. For example, Poe and Acrivos showed that, for $\mathrm{Re}_s > 0.6$, a sphere in shear flow rotates and the wake is oscillatory.[187] Similarly, the flow in the wake of a spinning sphere is unsteady and asymmetric, rendering extremely difficult the theoretical analysis or numerical simulation of the problem. Investigations of shear-generated lift beyond the near-Stokesian range are lacking, and evaluations of the Magnus lift force must be performed experimentally.[97]

In principle, the extension of Equations 15 and 16 to high-speed flows can be accomplished by rewriting them in terms of experimentally determined lift coefficients. For in-plane particle translational motion relative to a simply sheared fluid, with particle rotation and fluid vorticity aligned normal to this

plane, the equations for the moduli of the forces are

$$F_M = C_{LM}(\tfrac{1}{2}\rho_f U_r^2 \pi)\left(\frac{d_p}{2}\right)^2 \tag{17}$$

$$F_S = C_{LS}(\tfrac{1}{2}\rho_f U_r^2 \pi)\left(\frac{d_p}{2}\right)^2 \tag{18}$$

where U_r is the modulus of the particle average relative velocity. For the respective analyses of References 184 and 185, we find that

$$C_{LM} = \frac{\mathrm{Re}_r}{\mathrm{Re}_p} \tag{19}$$

$$C_{LS} = \frac{4.113\mathrm{Re}_s^{1/2}}{\mathrm{Re}_p} \tag{20}$$

At high Reynolds numbers, however, $C_{LM} = f(\mathrm{Re}_r/\mathrm{Re}_p, \mathrm{Re}_p)$. A summary of the experimental data available is provided in References 97 and 188. Corresponding measurements for C_{LS} at high Reynolds numbers apparently are unavailable.

Data for the drag coefficient, C_D, in the expression for the modulus of the drag force,

$$F_D = C_D(\tfrac{1}{2}\rho_f U_r^2 \pi)\left(\frac{d_p}{2}\right)^2 \tag{21}$$

for the case of spinning particles are also given in References 97 and 188. The data reveal an insensitivity of C_D to particle rotation. Ratios of C_{LM}/C_D obtained from these data show that the Magnus force is significant for all particles with $\mathrm{Re}_r/\mathrm{Re}_p > 1$, regardless of the value of Re_p.

Of special interest here are the effects of the Magnus and Saffman forces on the trajectories of particles striking and rebounding from solid surfaces at high speeds. For illustration, consider the flow of a particle-laden gas through a duct. In regions where $\mathrm{Re}_p \ll 1$, the ratio of the transverse forces is

$$\frac{F_M}{F_S} \propto \frac{d_p \Omega_p}{(\Omega_f \nu)^{1/2}} \tag{22}$$

which we can write as

$$\frac{F_M}{F_S} \propto \frac{d_p \Omega_p}{u_\tau} \tag{23}$$

where the relation $\Omega_f \nu \simeq \tau_w/\rho = u_\tau^2$ has been used. In turbulent duct flow we expect that

$$u_\tau \propto \frac{U_D^{7/8}\nu^{1/8}}{D^{1/8}} \tag{24}$$

where U_D is the mean velocity of the flow in the duct and D is the duct hydraulic diameter.[189] Substituting Equation 24 into Equation 23 and rearranging yields

$$\frac{F_M}{F_S} \propto \frac{d_p \Omega_p}{U_D}(\mathrm{Re}_D)^{1/8} \tag{25}$$

where $\mathrm{Re}_D = U_D D/\nu$ is the duct-flow Reynolds number. As $(\mathrm{Re}_D)^{1/8} = \mathrm{O}(1)$ for most duct flows of interest, we find that

$$\frac{F_M}{F_S} \propto \frac{d_p \Omega_p}{U_D} \tag{26}$$

If Ω_p is small, such as might be the case near but prior to impact, F_S is the dominant transverse force as a result of the shear acting on a particle. Upon rebounding, the particle may spin up but, because of viscous dissipation, $d_p\Omega_p < U_D$ and therefore $F_M < F_S$ again.

These findings pertain to $\mathrm{Re}_p \ll 1$, but they provide general guidance and suggest that in regions of strong shear, such as near walls, the Saffman force may be large relative to the Magnus force. Whether the Saffman force will significantly affect particle motion depends on shear-layer thickness. When it is thin, the trajectory of a rebounding particle that continues to spin after it emerges from the wall shear layer may be more strongly influenced by the *cumulative* action of the Magnus force. To show this effect, we consider that, according to Rubinow and Keller,[184] the characteristic time for an e^{-1} decrease in Ω_p resulting from viscous dissipation is

$$t_M \simeq \frac{d_p^2}{\nu} \tag{27}$$

For a shear layer of thickness δ, the characteristic time for the Saffman force is

$$t_S \simeq \frac{\delta}{U_{pn}} \tag{28}$$

where U_{pn} is the component of particle velocity normal to the shear layer. The ratio of these two time scales is

$$\frac{t_M}{t_S} \simeq \frac{d_p^2 U_{pn}}{\delta \nu} = \left(\frac{d_p}{D}\right)^2\left(\frac{D}{\delta}\right)\left(\frac{U_{pn}}{U_D}\right)\mathrm{Re}_D \tag{29}$$

From Reference 190, in a duct flow with $\mathrm{Re}_D = 10^5$, we find that $\delta/D \simeq 0.1$. If we assume that $U_{pn}/U_D \simeq 0.1$, then $t_M/t_S > 1$, provided that $d_p/D > 10^{-3}$. In practical terms, this finding would require that $d_p > 200\,\mu\mathrm{m}$ in a duct with $D = 0.2\,\mathrm{m}$, which is common in many particle-laden industrial flows.

The inclusion of $\vec{F}_M$ in the force balance for a particle makes it necessary to know how $\vec{\Omega}_p$ varies with time. For a spinning sphere, the conservation of angular momentum requires that

$$I\left(\frac{d\vec{\Omega}_p}{dt}\right) = -\vec{T} \tag{30}$$

where I is the moment of inertia of the sphere about any diameter, and $\vec{T}$ is the torque on the sphere from viscous effects. The appropriate expression for $\vec{T}$ depends on Re_p and Re_r. For $\mathrm{Re}_p \ll 1$ and all $\mathrm{Re}_r/\mathrm{Re}_p$, the analysis in Reference 184 gives

$$\vec{T} = -C_T \mu\left(\frac{d_p}{2}\right)^3 \vec{\Omega}_p \tag{31}$$

with $C_T = 8\pi$. For $250 < \mathrm{Re}_p < 550$ and $\mathrm{Re}_r/\mathrm{Re}_p \simeq 1$, Armstrong *et al.*[179] found $C_T = \mathrm{O}(100)$ for angular coal particles. For $550 < \mathrm{Re}_p < 1{,}600$ when $0.2 < \mathrm{Re}_r/\mathrm{Re}_p < 20$, Tsuji *et al.*[188] recommend the C_T correlation proposed in Reference 191. The solution of Equation 30 requires an initial value for the particle angular velocity, which usually is unknown. This unknown, combined with the uncertainty in C_T, renders the calculation of $\vec{\Omega}_p$—and hence of $\vec{F}_M$—rather inexact.[188]

Using a particle capture technique, Armstrong *et al.*,[179] demonstrated the importance of the Magnus force to erosion. They mapped the curved trajectories of angular coal particles approximately 150 μm in diameter rebounding from flat stainless steel and aluminum surfaces. The investigators took care to ensure stagnant fluid conditions in the vicinity of the target surfaces in order to minimize the effects of air motion on particle trajectories. The particle incidence speed ranged from 60 to 100 m s^{-1}, corresponding to $250 < \mathrm{Re}_p < 500$. Using a simplified analytical model, Armstrong *et al.* considered the behavior of the smaller particles for conditions typical of the gas turbine environment. From results such as those shown in Figure 12, they concluded that Magnus forces could affect the motions of 10-μm particles over rebound distances of about 20 mm. However, in estimating the initial particle angular velocity, they assumed that $U_p \simeq \Omega_p d_p/2$, implying that the translational energy of the particle is completely converted into rotational

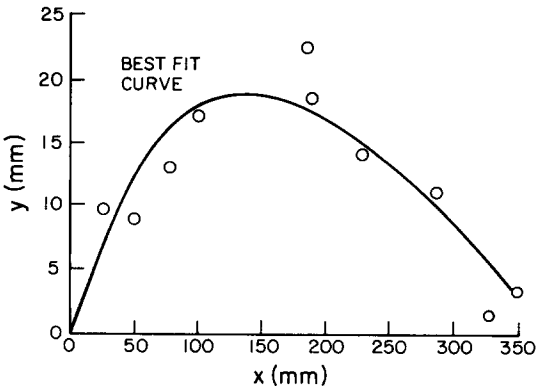

Figure 12 Best fit (line) to experimental data (circles) for the average trajectory of an angular coal particle rebounding with spin from an aluminum surface in a quiescent air environment. In the figure the x and y coordinates are parallel and perpendicular to the surface, respectively. The incidence particle velocity and angle were $V_1 = 140\,\mathrm{m\,s^{-1}}$ and $\beta_1 = 30°$, respectively. Based on measurements by Armstrong *et al.*[179]

energy. This assumption results in unrealistically large values of Ω_p.

Particle–wall collision phenomena in horizontal tubes at low volumetric concentrations of particles in a gas stream have been considered.[177] Individual particle behavior was examined under the assumption of 2-D particle motion. Analysis of particle collisions with the tube wall led to the conclusion that the dependence of particle trajectories on the Magnus force is more pronounced for conditions of adhesive friction than conditions of sliding friction. The reason is that, in the case of the former, the Magnus force changes sign with alternate wall impacts, because of the change in sign of a rebounding particle's spin. Consequently, the mean distance traveled by a particle between successive wall collisions is shorter and the energy lost by the particle to the wall is higher for conditions of adhesive friction.

3.3.4 *Particle–particle interactions near surfaces.* The presence of a solid surface substantially alters the nature of particle–particle interactions through the boundary constraint, and the rate of surface erosion can actually decrease with increasing particle concentration.[19,20] Uuemois and Kleis[20] suggested that collisions between particles approaching and leaving the surface impede the net advancement of particles moving toward the surface. According to them, the collisions create a protective barrier that reduces erosion. A similar argument has been proposed to explain concentration-dependent erosion results for high-temperature hypersonic flows.[192] That the frequency of such interparticle collisions is favored at high levels of flux seems reasonable, but little seems to be known about the collision process itself. This lack of knowledge is not surprising, in view of the difficulty of measuring or modeling the random, 3-D interactions among particles advancing toward, and rebounding from, a surface undergoing erosion in turbulent flow.

Under idealized conditions, however, useful analytical results can be derived. Andrews and Horsfield[36] have done so for conditions corresponding to a monodisperse stream of spherical particles traveling along initially parallel trajectories toward a flat surface. Their analysis is limited to low particle concentrations (low flux) and—because it ignores fluid friction effects—is limited to relatively inertial particles ($\lambda \gg 1$). Andrews and Horsfield further assumed that, in the absence of collisions among particles approaching the surface and particles leaving the surface, all particles approach the surface at velocity V_1 and angle β_1 and, upon rebounding, leave the surface at velocity V_2 and angle β_2. For these conditions they derived an expression for the mean free path, λ_m, of a particle approaching the surface before colliding with a particle leaving the surface:

$$\lambda_m \simeq \frac{2V_1V_2}{\pi d_p \Omega_1 \Omega_2} \cos^2(\alpha/2) \tag{32}$$

In this expression, $\alpha = \pi - \beta_1 - \beta_2$, and the Ωs are the frequencies of spheres moving along an approaching trajectory (Ω_1) or departing trajectory (Ω_2) with respect to the surface.

If we assume elastic collisions and that $\beta_1 = \beta_2$, the expression for λ_m becomes

$$\lambda_m \simeq d_p^{-5} N_p^{-2} \cos^2(\pi/2 - \beta_1) \tag{33}$$

where N_p is the number of particles per unit volume in the flow. Requiring that an approaching particle travel a distance λ_m with angle β_1 prior to collision, Equation 33 provides a relation between particle size and concentration. Of course, this result is specific to the sandblast type of flow configuration idealized by Andrews and Horsfield and is subject to the assumptions mentioned.

Relations describing the self-scattering of a dilute ensemble of moving spheres for the sandblast configuration are also described in Reference 36. Scattering was modeled by presuming elastic collisions between pairs of spheres, the orientation of which at the instant of impact was taken to be random. From the results for the relative energy of the scattered spheres as a function of scatter angle, two especially interesting observations emerge: (1) except for a very small fraction of spheres, one of each pair of spheres that collide returns to strike the surface, the second sphere having a finite probability of doing likewise; and (2) because the orientation angle between colliding spheres is presumed to be random, a distribution of possible particle speeds and trajectories for the particles both approaching and those leaving the surface exists.

The first point is significant in that it supports the idea that interparticle collisions at low levels of flux *do not necessarily reduce* the number of particles striking a surface. It contradicts the notion that a protective barrier can be set up at a surface through interparticle collision, as suggested by Uuemois and Kleis.[20] Instead, we can argue that collisions reduce the energy content of approaching particles by transmitting some of this energy to particles rebounding from the surface. Thus, even though the number of surface impacts will increase with increasing particle concentration in a constant-speed jet sandblast, the energy per particle is less, thus resulting in less damaging impacts and reduced wear.

The second point suggests the interesting possibility of nonuniform surface erosion caused by the redirection of particles as a consequence of collision. Thus, for example, a stream of particles approaching a ductile surface at about $\beta_1 = 25°$ should produce maximum wear.[6] However, the analysis in Reference 36 shows that, because of particle redirection, erosion must be integrated over jet blast angles ranging from 0° to 50°, approximately. The opposite is also possible: that particles initially directed along nondamaging trajectories can, as a result of collision, be redirected along potentially more erosive routes.

In spite of the relative simplicity of their analysis, which is devoid of fluid mechanics effects, experiments performed by Andrews and Horsfield with fairly inertial particles appear to support some of their theoretical predictions. The motions of large glass spheres striking a target of variable inclination angle were investigated photographically. The spheres had $d_p \simeq 600\,\mu\mathrm{m}$ and a speed of $13 \pm 1\,\mathrm{m\,s^{-1}}$. The incidence angle was varied over the range $20° < \beta_1 < 50°$. The average flux of spheres investigated experimentally was 0.03–0.3 $\mathrm{gr\,cm^{-2}\,s^{-1}}$, and was within the low-flux limit of the analysis. Unfortunately, the majority of the collisions observed in the experiment were

between fast arriving spheres and slow stray spheres, which affected the results and their interpretation. Whether the same observations would apply to particles in the range of 1–100 μm striking solid surfaces in the presence of strong turbulence effects remains to be seen. The corresponding problem of *indirect* particle–particle interactions modulated by the presence of a solid surface has not been investigated extensively.

Idealized approaches to analyzing particle–particle collisions are useful, but future efforts must emphasize the simulation of more realistic conditions. Future analyses and experimentation should include the investigation of (a) interactions among particles of differing sizes, densities, and shapes; (b) particle rotation (prior to and as a consequence of collision); (c) nonelastic collision conditions; (d) 3-D conditions; (e) influence of the flow field, particularly near-wall turbulence; (f) high particle concentrations; and (g) particle fragmentation.

3.3.5 *Surface topography.* The result of erosion by particle impact is alteration of the surface's topography. Cracks, grooves, and craters with raised edges, scales, etc., are the product of multiple and irregular particle–surface collisions. Scarring of the material's surface at the microscopic level has a random appearance, but large-scale patterns and regularly spaced ripples have been observed.[13,193]

A study by Scattergood and Routbort,[194] using 37-μm and 270-μm diameter Al_2O_3 particles impacting perpendicularly on (111) silicon single-crystal surfaces at 210 m s^{-1} shows that the initial transient in the weight-loss curve depends on the condition of the surface prior to erosion. If the surface is pre-eroded by particles larger than those used subsequently, a decelerating transient is observed. An accelerating transient is observed when pre-erosion is conducted with particles smaller than those used subsequently. Scattergood and Routbort explained their results by comparing the length of the subsurface flaws with that of the impacting particles. If the characteristic scale of the subsurface flaws is smaller than that corresponding to the impacting particle, the transient accelerates and vice versa. Gulden has made similar observations.[195]

Experiments[22] on the time-dependence of plexiglass erosion by 10- and 30-μm diameter alumina particles at speeds of 84 and 65 m s^{-1}, respectively, show that $E \propto t^c$, with $c = -0.1$. The parameter c is a system constant and was found to be independent of particle speed, incidence angle, and particle size. The decrease in erosion with time was attributed, in part, to increasing surface roughness but, as in Reference 194, the explanation offered was entirely within the context of a mechanism for erosion: "It can be seen that after a few seconds of erosion the surface is considerably roughened and that particle impingement is no longer occurring at a normal angle of impingement." In fact, at an exposure time of about 120 s, the *effective* particle–surface incidence angle was about 55°, and we know that for brittle materials a departure from a normal incidence angle reduces erosion.[4]

For both brittle and ductile materials, the evolution of surface topography is important. Observable surface changes caused by material removal form the basis for hypothesized mechanisms of erosion as, for example, in the platelet mechanism of erosion for ductile metals.[196–198] If erosion is accompanied by corrosion, the formation of corrosion scale may enhance or inhibit erosion, depending on the depth of the particle's cut, the rate and nature of scale growth, and the adhesiveness of the scale to the surface.

These studies focused on the role of surface roughness in mechanisms for explaining erosion. Except for the interesting turbulent flow study of Mason and Smith,[165] little attention has been given to the synergistic effects between erosion-induced surface-evolving topographies and the associated fluid motion. The study reported in Reference 165 centered on large-scale changes in the topography of bends. However, the local influence of surface roughness on fluid and particle motions was not investigated. We will discuss this topic briefly.

The *wall region* of a developed turbulent flow is characterized by a large spectrum of scales of motion and vigorous unsteady dynamics.[199] However, the average velocity component, U_f, of fluid moving parallel to a solid surface can be expressed as

$$\frac{U_f}{u_\tau} = \frac{1}{\kappa} \ln\left(\frac{y u_\tau}{\nu}\right) + f\left(\frac{h u_\tau}{\nu}\right) \tag{34}$$

where u_τ is the wall friction velocity, defined earlier, y is the normal distance from the surface, h is the "equivalent" roughness height and κ is the von Karman constant. The wall region to which Equation 34 applies is bounded by $40\nu/u_\tau < y < 0.2\delta$, where δ is the boundary-layer thickness. For values $hu_\tau/\nu > 5$, the roughness has the effect of reducing the mean fluid velocity relative to that which would develop along a smooth wall, and for $hu_\tau/\nu > 70$, this effect becomes pronounced. Appropriate forms for the function $f(hu_\tau/\nu)$ in Equation 34 are summarized in Reference 200.

For a pipe flow at room temperature with $Re_D = 10^5$, the magnitude of the friction velocity is $u_\tau = O(10\,m\,s^{-1})$. Thus roughness elements of height $h > 100\,\mu$m in air or $h > 10\,\mu$m in water significantly reduce the mean speed of fluid near a surface (relative to a smooth surface) at this value of Re_D. Photographic evidence suggests that typical values of h for surfaces roughened by particle impacts range from 1 to 1,000 μm. Because of viscous damping in the sublayer region of the flow, fluids with high kinematic viscosity, ν, are less sensitive than fluids with low ν to the presence of protrusions on a surface. However, in both cases the roughness retards the mean component of fluid motion and hence particle motion parallel to the surface.

The ultimate consequences for erosion owing to surface roughness are hard to generalize, because particle-incidence speeds and angles that determine the amount and spatial distribution of surface wear depend markedly on λ and local flow turbulence. Nevertheless, relative to a smooth pipe, we can reasonably expect that, in an initially rough pipe, particles with $\lambda > 1$ approaching the pipe wall at shallow erosive angles on average will be deviated less from their damaging trajectories by the component of fluid motion parallel to the wall.

Even from such a crude picture, based on a mean-flow interpretation of a region of flow characterized by intense velocity fluctuations distributed randomly in time and over space, we must conclude that roughness elements can alter both the magnitude and topography of surface erosion by affecting the flow. Investigators must consider such a possibility when planning experiments and interpreting observations or when attempting to calculate the trajectories of particles near a surface.

3.4 *Temperature effects*

Several investigators have argued that localized high-temperature conditions created by high-speed particle impacts can soften and even melt metal surfaces at the impact locations.[33,201] On this point there are two views: (1) the fundamental mechanisms governing erosion are mechanical, so if thermal phenomena favor erosion the effect is small; and (2) thermal phenomena, namely melting, can significantly increase erosion. Prior to discussing some of the main studies addressing these two points of view, we must note that many of the studies involved the use of relatively large particles [$d_p = O(1\,mm)$] to induce the thermal effects observed. Whether the observations reported also apply to smaller particles [$d_p = O(10\,\mu m)$], which are more likely to occur in erosive flows, is yet to be established through rigorous similarity consideration and experimentation.

Some investigators claim that metal softening and localized shear deformation facilitate the formation of deep craters with extended edges from which metal pieces break off easily during subsequent impacts.[20,23,202] High-speed photographs of the impacts of steel spheres projected obliquely onto mild steel targets show that target material is detached along a band of intense subsurface shear.[203] Calculations of the phenomenon, based on an energy balance on the sphere, show that it is associated with the high temperatures induced locally by the impacts. Other investigators argue that at high-impact speeds a rapid process of metal melting–resolidification can take place at the particle–metal interface.[47,201,204–206] In this model, as the particle rebounds it removes solidified metal material which has adhered to its surface. This mechanism is favored when target surfaces are already at high temperatures.

Against the melting-enhanced erosion arguments are the observations that high temperatures can increase metal ductility, facilitate particle embedding, and produce oxide films. A sufficiently ductile metal will allow a grazing particle to plow along its surface, moving material to either side of the grove, without actually removing material from the surface. Oxide films and embedded particles can work to shield a surface from subsequent damaging particle impacts. However, the results concerning embedding are inconclusive. For example, although embedding significantly reduces particle deposition on the surface,[183] much of the erosion data available suggests that embedding does not inhibit wear significantly.[33]

These studies pertain to localized temperature effects produced by particles striking surfaces at high speed. The response of erosion to controlled variations of target temperature has also been investigated.[11,18,31,170,201,207] Andrews and Field[201] measured the wear of annealed copper targets impacted by 5-mm diameter hardened steel spheres at speeds ranging from 110 to 150 m s^{-1}. They performed the experiments in a non-oxidizing (argon gas) environment and showed that erosion increased with increasing target temperature over the range 800–1,400°K. However, they note that the mass losses may have been affected by additional temperature increases at the places of particle impact.

Experiments conducted in more realistic corrosive environments yield contrasting results. For example, Ganesan *et al.*[208] measured room-temperature erosion by 30-μm alumina particles of 304 and 310 stainless steel specimens previously exposed to a gas mixture of 1% H_2S in N_2 at 600°C, 700°C, and 800°C, respectively. They attribute the differences observed in the erosion behavior of specimens corroded at different temperatures to differences in the nature of the scales formed. At low temperature the scales were crystalline and weakly adherent, whereas at high temperatures they were more strongly adherent but appeared to be more brittle. Nevertheless, corroded specimens always showed greater initial rates of erosion relative to uncorroded specimens.

By contrast, Young and Ruff[170] observed that the erosion of various types of stainless steel by 5- and 50-μm Al_2O_3 particles in a gas jet is less at 500°C than at 25°C. They attributed the reduction in erosion to the better protection afforded by the thicker oxide coating formed at 500°C. They attributed the comparatively smaller reduction in erosion for the case of the 50-μm particles to the particle's depth of cut being larger than the thickest oxide scale thickness formed, which therefore offered little protection. However, their interpretation is confounded by particle-motion considerations that also reduce erosion at high temperatures. Dosanjh and Humphrey[39] analyzed a similar configuration. They calculated the flows of particle-laden gas jets aimed at flat surfaces. They showed that increasing the carrier gas temperature (as Young and Ruffs did, to 300°C for the runs with the specimens at 500°C) decreases the particle incidence speed (V_1) and incidence angle (β_1), as well as the particle flux (F_1) to the surface. We can readily explain the reason for this result in fluid mechanics terms by noting that the ratio of momentum equilibration numbers at the same location between two flow configurations, I and II, that differ only in temperature and particle size is

$$\frac{\lambda_I}{\lambda_{II}} = \frac{\mu_{II}}{\mu_I}\left(\frac{d_{pI}}{d_{pII}}\right)^2 \tag{35}$$

If $d_{pI} = d_{pII}$, and we assume that $\mu \propto T^{1/2}$ (ideal gas), then:

$$\frac{\lambda_I}{\lambda_{II}} \propto \left(\frac{T_{II}}{T_I}\right)^{1/2} \qquad \text{(temperature effect on } \lambda) \tag{36}$$

However, if $T_I = T_{II}$ but $d_{pI} \neq d_{pII}$, then:

$$\frac{\lambda_I}{\lambda_{II}} \propto \left(\frac{d_{pI}}{d_{pII}}\right)^2 \qquad \text{(particle size effect on } \lambda) \tag{37}$$

Therefore small values of λ—characteristic of particles that closely follow the fluid motion and tend not to strike the surface—tend to result from increased gas-stream temperature, and the tendency is strengthened by reducing particle size. In particular, from Equation 35, we expect very large differences in erosion between 5-μm particles in a gas jet at 300°C and 50-μm particles in a gas jet at 25°C (as observed by Young and Ruff), *independently of oxide scale considerations.*

Young and Ruff explain yet another interesting feature of their observations in terms of the oxidation scales formed on the materials investigated, but which admits a purely fluid mechanics interpretation. Figure 13[170] shows that erosion by 50-μm particles at 500°C is less than that at 25°C. In addition, relative to the results at 25°C, the results at 500°C are displaced towards smaller particle-incidence angles[1]. This result means that particles of a fixed size with small incidence angles and in streams at high temperature and identical particles having larger incidence angles in streams at low temperature will erode equivalently. That this is the expected result can be shown using the cutting model proposed by Finnie[6] and the numerical fluid mechanics results obtained by Dosanjh and Humphrey.[39] For incidence angles of $18.5° < \beta_1 < 90°$, the cutting model yields

$$E \propto F_1 V_1^2 \cos^2 \beta_1 \tag{38}$$

For two identical flow configurations, I and II, that differ only in temperature, $E_I = E_{II}$ when

$$(F_1 V_1^2 \cos^2 \beta_1)_I = (F_1 V_1^2 \cos^2 \beta_1)_{II} \tag{39}$$

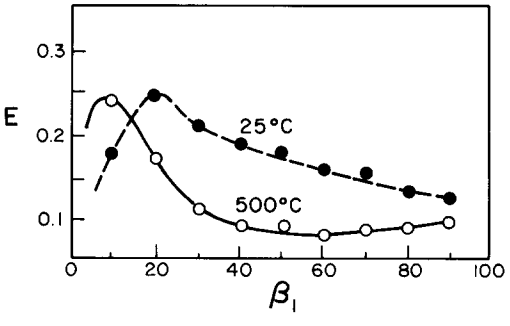

Figure 13 Erosion of an isothermal surface by a particle-laden jet of CO_2 gas as a function of the blast jet incidence angle. Conditions correspond to a stainless steel target at two temperatures impacted by Al_2O_3 particles of diameter 50 μm at a speed of 30 m s^{-1}. Based on measurements by Young and Ruff[170]

[1] In the absence of experimental values, the particle-incidence angle is assumed to be proportional to the acute angle formed by the gas jet and the target surface.

The results reported in Reference 39 show that, generally, $(F_1V_1^2)_{1,200K}/(F_1V_1^2)_{300K} < 1$ for the range of β_1 of interest here. It follows from Equation 39 that $(\cos\beta_1)_{300K} < (\cos\beta_1)_{1,200K}$ and therefore that $(\beta_1)_{300K} > (\beta_2)_{1,200K}$. The conclusion is that the incidence angles of particles in a cold gas stream *must be larger* than those of identical particles in a hot stream to attain the same rates of erosion. This interpretation of the data in Figure 13 does not necessarily imply that Young and Ruff's protective oxide film hypothesis[170] is incorrect. The only conclusions to be drawn here are that (a) both interpretations are valid, but there is insufficient information available from this or any other experiment to rank them in order of importance; and (b) thermally induced viscous effects can significantly affect particle motion and hence erosion in gas–solid flows.

Unfortunately, in oxidizing and other corrosive environments, clear and generally applicable interpretations of the effects of temperature on erosion are difficult to formulate. The synergistic effects between the two modes of mass loss are complex, insufficiently documented, poorly understood, and, as a result, difficult to model. Hogmark *et al.*[209] pointed out that no material has yet been completely characterized in terms of its corrosion/erosion behavior, which includes knowing (a) the corrosion and erosion properties of the base material; (b) the erosion properties of the corroded surface layer; and (c) the erosion properties of the base material coated with a corroded layer, in particular the dynamics of the particle–corrosion-layer interaction especially when the corrosion layer takes the form of a flaky material of poorly defined properties and mechanical behavior. Hence, for most systems of practical interest, fluid mechanics (turbulence especially) plays a critical role. The reason is that many surface corrosion reactions are diffusion controlled. The rates at which chemical species and particles with $\lambda < 1$ approach or leave a surface ultimately depend on the large-scale convective motion that transport them between regions near the surface and the bulk of the flow and on the interaction of the flow with the surface, which may be smooth or rough. In this regard, corrosion scales can behave like roughness elements and will affect the transport process. There is a considerable body of literature on corrosion and, increasingly, more studies are appearing on the subject of erosion–corrosion.[24,209–221]

4. Conclusions

Particle-laden fluids are responsible for costly erosion problems that are of grave concern to many important industries. We need to understand and control erosion for economic, safety, and resource conservation reasons. Certainly, with direct and indirect losses sustained by industry and the military amounting to hundreds of millions of dollars annually, the primary motivation for understanding and controlling erosion is economic.

This review focused on uncovering and discussing various, previously neglected, fundamental issues of the role played by fluid mechanics in erosion caused by the impact of solid particles. We emphasized understanding physical phenomena, which could, in principle, lead to improved control of particle motion in order to eliminate, or at least minimize, wear. The review led to several major conclusions.

(1) There are numerous instances in the erosion literature, a few of which were discussed here, of findings that have been attributed to materials-related causes but which admit purely fluid mechanics interpretations.

(2) Previous experimental work in erosion has failed to adequately control, let alone measure with any degree of accuracy, the fluid mechanics variables that affect solid particle motion and surface impact. The variables include the instantaneous velocities of the fluid and particle phases, especially near the surfaces undergoing erosion, and temperature in nonisothermal flows.

(3) In relation to conclusion 2, no fundamental experimental study of erosion by particle impact has yet been undertaken in which the characteristics of the turbulence are varied in a controlled and systematic manner over a meaningful range of the relevant parameters. The experimental methodologies exist, and conducting such investigations is imperative. They can provide the data (and uncertainty bounds) so necessary for guiding and testing mathematical model developments that will render erosion predictable in systems of interest to industry.

(4) In his review, Leschziner[79] concluded that computational fluid dynamics has reached the stage where it can be applied almost routinely to many single-phase flows in highly complex 3-D geometries typical of industrial processes. Even though problems remain, they are solvable, as recent research has shown. However, direct numerical simulations of turbulent flows are unlikely to benefit industry in the immediate future, and phenomenological modeling approaches will continue to be the workhorse predictors of turbulent flows in complex configurations. Extensions of single-phase phenomenological models to two-phase flows have already been undertaken, and some were discussed here. For purposes of modeling erosion by solid particle impact, Lagrangian formulations of the particle phase are preferred to Eulerian formulations. The former are based on application of a physically intuitive force balance to the particle, which explicitly allows, for example, the inclusion of lateral forces that can markedly alter the trajectory of a particle near a surface. In this regard, significant progress has been made in the modeling of monodispersed dilute systems in which particles collide infrequently among themselves in the bulk of the flow or near the surface undergoing erosion. However, the corresponding behavior of more realistic concentrated polydispersed particle–gas flows has yet to be modeled satisfactorily, especially near surfaces.

(5) Many important aspects of the erosion process are, at present, too complex to model, and accurate direct measurements of them are probably impossible. They relate to particle–particle collisions and particle–surface interactions, such as rebounding, fragmentation, and spin. Innovative experimental and theoretical approaches are sorely needed. However, they must be tempered by weighing the benefits of developing procedures aimed at measuring or computing details against the value of establishing simpler but proven approaches that will provide results quickly and with acceptable uncertainties.

(6) Ultimately, the prediction of wear by particle impact must rely on the formulas derived by materials scientists for calculating erosion. Much of the early work in this area was experimental, consisting primarily of establishing empirical correlations describing the erosion (often accelerated) of very specific pairs of materials for very specific experimental conditions. As a result, little that is universally applicable has emerged. More recently, significant theoretical advances have been made in the materials area (not reviewed here) that show promise for the development of more generally applicable erosion equations. However, such research cannot be concluded successfully without close scrutiny and control of the fluid mechanics aspects of erosion. In this regard, effective technical communication between materials scientists and fluid mechanicists is indispensable.

Acknowledgments

This review was motivated by the pioneering work of J. A. Laitone on the effects of fluid motion in erosion by solid particle

impact. Special thanks go to I. Cornet and A. Levy who introduced me to the subject. Partial support for the review and related ongoing research in Berkeley has been provided by the Assistant Secretary for Fossil Energy Research, University Coal Research Division, U.S. Department of Energy, under Contract No. DE-AC03-76SF00098, and by Martin Marietta through subcontract No. 19X-55936C, under a prime contract from the Department of Energy. I am grateful for this support and to S. Dapkunas, R. Judkins, and P. Carlson for their interest in the work. Finally, I am indebted to the secretarial staff of the Department of Mechanical Engineering, in particular M. A. Peters and C. Schoon, for the competence and patience they displayed in preparing this manuscript.

References

1 Zahavi, J. and Schmitt, G. F. Solid particle erosion of reinforced composite materials. *Wear*, 1981, **71**, 179–190
2 Zahavi, J. and Schmitt, G. F. Solid particle erosion of polymeric coatings. *Wear*, 1981, **71**, 191–210
3 Zahavi, J. and Schmitt, G. F. Solid particle erosion of coatings on transparent polycarbonate and reinforced composites. *Selection and Use of Wear Tests for Coatings*, ASTM STP 769 (R. G. Bayer, Ed.), American Society for Testing and Materials, 1982, 28–70
4 Adler, W. F. Assessment of the state of knowledge pertaining to solid particle erosion. Final Report, No. CR79-680, to the U.S. Army Research Office for contract DAAG29-77-C-0039, 1979
5 Finnie, I. The mechanism of erosion of ductile metals. *Proc. 3rd U.S. National Congress of Applied Mechanics*, Pergamon Press, London, 1958, 527–532
6 Finnie, I. An experimental study of erosion. *Proc. Soc. Exptl. Stress Anal.*, 1960, **17**(2), 65–70
7 Finnie, I. Erosion of surfaces by solid particles. *Wear*, 1960, **3**, 87–103
8 Finnie, I. Some observations on the erosion of ductile metals. *Wear*, 1972, **19**, 81–90
9 Finnie, I. On the velocity dependence of the erosion of ductile metals by solid particles at low angles of incidence. *Wear*, 1978, **48**, 181–190
10 Finnie, I. and McFadden, D. H. On the velocity dependence of the erosion of ductile metals by solid particles at low angles of incidence. *Wear*, 1978, **48**, 181–190
11 Finnie, I., Levy, A., and McFadden, D. H. *Fundamental Mechanisms of the Erosive Wear of Ductile Metals by Solid Particles, Erosion: Prevention and Useful Applications*, ASTM STP 664 (W. F. Adler, Ed.), American Society for Testing and Materials, 1979, 36–58
12 Finnie, I. The mechanisms of erosive wear in ductile metals. *Corrosion-Erosion Behavior Materials* (K. Natesan, Ed.), Metallurgical Society of AIME, 1980, 118–126
13 Bitter, J. G. A. A study of erosion phenomena (Part 1). *Wear*, 1963, **6**, 5–21
14 Bitter, J. G. A. A study of erosion phenomena (Part 2). *Wear*, 1963, **6**, 169–190
15 Sheldon, G. L. and Finnie, I. On the ductile behavior of nominally brittle materials during erosive cutting. *J. Eng. Ind.*, Nov. 1966, 387–392
16 Sheldon, G. L. and Finnie, I. The mechanism of material removal in the erosive cutting of brittle materials. *J. Eng. Ind.*, Nov. 1966, 393–400
17 Neilson, J. H. and Gilchrist, A. Erosion by a stream of solid particles. *Wear*, 1968, **11**, 11–122
18 Neilson, J. H. and Gilchrist, A. An experimental investigation into aspects of erosion in rocket motor tail nozzles. *Wear*, 1968, **11**, 123–143
19 Tilly, G. P. and Sage, W. The interaction of particle and material behavior in erosion processes. *Wear*, 1970, **16**, 447–465
20 Uuemois, H. and Kleis, I. A critical analysis of erosion problems which have been little studied. *Wear*, 1975, **31**, 359–371
21 Sage, W. and Tilly, P. The significance of particle size in sand erosion of small gas turbines. *Aero. J. Royal Aero. Soc.*, 1969, **73**, 427–428
22 Sargent, G. A., Mehrota, P. K., and Conrad, H. A model for the multiparticle erosion of brittle solids by spherical particles (Paper No. 28). *Proc. 5th Int. Conf. on Erosion by Liquid and Solid Impact* (J. E. Field, Ed.), Cambridge, England, 1979
23 Hutchings, I. M. Mechanisms of the erosion of metals by solid particles. *Erosion: Prevention and Useful Applications*, ASTM STP 664 (W. F. Adler, Ed.), ASTM, 1979, 59–76
24 Hutchings, I. M. Recent advances in the understanding of solid particle erosion. *Mecanique, Materiaux, Electricite*, 1980, **365**, 185–192
25 Hutchings, I. M. A model for the erosion of metals by spherical particles at normal incidence. *Wear*, 1981, **70**, 269–281
26 Andrews, D. R. An analysis of particle erosion mechanisms. *J. Phys. D: Appl. Phys.* 1981, **14**, 1979–1991
27 Söderberg, S., Hogmark, S., Engman, U., and Swahn, H. Erosion classification of materials using a centrifugal erosion tester. *Tribology International*, 1981, 333–344
28 Söderberg, S., Hogmark, S., and Swahn, H. Mechanisms of material removal during erosion of a stainless steel. Paper No. 82-AM-4A-1, 37th ASLE Annual Meeting, Cincinnati, May 10–13, 1982
29 Mills, D. and Mason, J. S. Learning to live with erosion of bends (Paper G1). *Proc. First Int. Conf. on the Internal and External Protection of Pipes*, University of Durham, Sept. 9–11, 1975, G1-1–G1-19
30 *Erosion: Prevention and Useful Applications*, (W. F. Adler, Ed.) ASTM STP 664, Philadelphia, 1979
31 Tilly, G. P. Erosion caused by impact of solid particles. *Treatise on Materials Science and Technology*, Vol. 13, Academic Press, 1979
32 Schmitt, G. F. Liquid and solid particle impact erosion. *Wear Control Handbook* (M. B. Peterson and W. O. Winer, Eds.), ASME, New York, 1980, 231–282
33 Shewmon, P. G. and Sundarajan, G. The erosion of metals. *Ann. Rev. Mat. Sci.*, 1983, **13**, 301–318
34 Cousens, A. K. and Hutchings, I. M. A critical study of the erosion of an aluminum alloy by solid spherical particles at normal impingement. *Wear*, 1983, **88**, 335–348
35 Laitone, J. A. Aerodynamic effects in the erosion process. *Wear*, 1979, **56**, 239–246
36 Andrews, D. R. and Horsfield, N. Particle collisions in the vicinity of an eroding surface. *J. Phys. D: Appl. Phys.*, 1983, **16**, 525–538
37 Laitone, J. A. Erosion prediction near a stagnation point resulting from aerodynamically entrained solid particles. *J. Aircraft*, 1979, **16**, 809–814
38 Laitone, J. Characterization of particle rebound phenomena in the erosion of turbomachinery. *J. Aircraft*, 1983, **20**, 275–281
39 Dosanjh, S. and Humphrey, J. A. C. The influence of turbulence on erosion by a particle-laden fluid jet. *Wear*, 1985, **102**, 309–330
40 Youngdahl, C. A. and Ellingson, W. A. Acoustic system for monitoring pressure boundary wear. Presented at the Symposium on Instrumentation and Control for Fossil Energy Processes, Houston, June 7–9, 1982
41 Hutchings, I. M. Introduction to the microscopy of erosion. *J. Microscopy*, 1983, **130**, 331–338
42 Andrews, D. R. A gravity-insensitive technique for measuring mass changes in hostile environments, including erosion. *J. Phys. E: Sc. Instr.*, 1983, **16**, 803–806
43 Thomas, G. P. The initial stages of deformation in metals subjected to repeated liquid impact. *Phil. Trans. Roy. Soc. A*, 1966, **260**, 140
44 Ives, L. K. and Ruff, A. W. Transmission and scanning electron microscopy studies of deformation at erosion impact sites. *Wear*, 1978, **46**, 149–162
45 Ives, L. K. and Ruff, A. W. Electron microscopy study of erosion damage in copper. *Erosion: Prevention and Useful Applications*, (W. F. Adler, Ed.) ASTM STP 664, 1979, 5–35
46 Brainard, W. A. and Salik, J. Scanning-electron-microscope study of normal-impingement erosion of ductile metals. NASA TP 1609, Lewis Research Center, Cleveland, 1980

47 Brainard, W. A. and Salik, J. An investigation into the role of adhesion in the erosion of ductile metals. *ASLE Trans.*, 1980, **24**, 302–306

48 Ruff, A. W. and Ives, L. K. Measurement of solid particle velocity in erosive wear. *Wear*, 1975, **35**, 195–199

49 Ponnaganti, V., Stock, D. E., and Sheldon, G. L. Measurement of particle velocities in erosion processes. *Symp. on Polyphase Flow and Transport Technology* (R. A. Bajura, Ed.), ASME, Century 2—Engineering Technology Conferences, 1980, 217–222

50 Sheldon, G. L., Maji, J., and Crowe, C. T. Erosion of a tube by gas-particle flow. *J. Eng. Mater.*, 1977, **99**, 138–142

51 Chigier, N. A. Velocity measurements of particles in sprays (Paper No. 1-4-30). *Symp. on Flow—Its Measurement and Control in Science and Industry*, Pittsburgh, May 1971

52 Hutchings, I. M. Erosion of metals by solid particles—Study using high-speed photography. BK No. 01318, 1977, 358–361

53 Van Horn, G. R. Rotating drum cameras for high speed photography. *Electro-Optical Systems Design*, 1977, 26–29

54 Meynart, R. Speckle velocimetry study of vortex pairing in a low-Re unexcited jet. *Phys. Fluids*, 1983, **26**, 2074–2079

55 Meynart, R. Instantaneous velocity field measurements in unsteady gas flow by speckle velocimetry. *Appl. Optics*, 1983, **22**, 535–540

56 Durst, F., Melling, A., and Whitelaw, J. H. *Principles and Practice of Laser-Doppler Anemometry*, Academic Press, London, 1976

57 Drain, L. E. *The Laser-Doppler Technique*, John Wiley and Sons, New York, 1980

58 Dring, R. P. Sizing criteria for laser anemometry particles. *J. Fluids Eng.*, 1982, **104**, 15–17

59 Einav, S. and Lee, S. L. Measurement of velocity distributions in two-phase suspension flows by the laser-Doppler technique. *Rev. Sci. Instrum.*, 1973, **44**, 1478–1480

60 Durst, F. and Zare, M. Laser-Doppler measurements in two-phase flows. *Proc. LDA-Symp.*, University of Denmark, Copenhagen, 1975, 403–429

61 Yule, A. J., Chigier, N. A., Atakans, S., and Ungut, A. Particle size and velocity measurements by laser anemometry. *J. Energy* 1977, **1**(4), 220–228

62 Ungut, A., Yule, A. J., Taylor, D. S., and Chigier, N. A. Particle size measurement by laser anemometry. *J. Energy*, 1978, **2**(6), 330–336

63 Lee, S. L. and Srinivasan, J. Measurement of local size and velocity probability density distributions in two-phase suspension flows by laser-Doppler technique. *Int. J. Multiphase Flow*, 1978, **4**, 141–155

64 Lee, S. L. and Srinivasan, J. An LDA technique for in situ simultaneous velocity and size measurement of large spherical particles in a two-phase suspension flow. *Int. J. Multiphase Flow*, 1982, **8**, 47–57

65 Durst, F. Review-combined measurements of particle velocities, size distributions, and concentrations. *J. Fluids Eng., Trans. ASME*, 1982, **104**, 284–296

66 Tsuji, Y., Morikawa, Y., and Shiomi, H. LDV measurements of an air-solid two-phase flow in a vertical pipe. *J. Fluid Mech.*, 1984, **139**, 417–434

67 The accuracy of flow measurements by laser-Doppler methods. *Proc. LDA-Symp.* (P. Buchave, J. M. Delhaye, F. Durst, W. K. George, K. Refslund, and J. H. Whitelaw, Eds.), Copenhagen, 1976

68 Buchave, P., George, W. K., and Lumley, J. L. The measurement of turbulence with the laser-Doppler anemometer. *Ann. Rev. Fluid Mech.*, 1979, **11**, 443–503

69 Laser velocimetry and particle sizing. *Proc. Third Int. Workshop on Laser Velocimetry* (H. D. Thompson and W. H. Stevenson, Eds.), Purdue University, Hemisphere Publishing Corporation, 1979

70 *Proc. First Int. Symp. on Applications of Laser-Doppler Anemometry to Fluid Mechanics* (R. J. Adrian, D. F. G. Durao, F. Durst, H. Mishina and J. H. Whitelaw, Eds.), Lisbon, 1982

71 *Proc. Second Int. Symp. on Applications of Laser-Doppler Anemometry to Fluid Mechanics* (R. J. Adrian, D. F. G. Durao, F. Durst, H. Mishina and J. H. Whitelaw, Eds.), Lisbon, 1984

72 *Proc. Third Int. Symp. on Applications of Laser-Doppler Anemometry to Fluid Mechanics*, (R. J. Adrian, D. F. G. Durao, F. Durst, H. Mishina and J. H. Whitelaw, Eds.), Lisbon, 1986

73 Tabakoff, W. and Sugiyama, Y. Experimental method of determining particle restitution coefficients. *Proc. Symp. on Polyphase Flow and Transport Technology* (R. A. Bajura, Ed.), ASME, Century 2—Engineering Technology Conferences, 1980, 203–210

74 Tennekes, H. and Lumley, J. L. *A First Course in Turbulence*, MIT Press, Cambridge, Massachusetts, 1972

75 Reynolds, W. Computation of turbulent flows. *Ann. Rev. of Fluid Mech.*, 1976, **8**, 183–208

76 *Handbook of Turbulence, Vol. I: Fundamentals and Applications* (W. Frost and T. H. Moulden, Eds.), Plenum Press, New York, 1977

77 Bradshaw, P., Cebeci, T., and Whitelaw, J. *Engineering Calculation Methods for Turbulent Flow*, Academic Press, London, 1981

78 *Topics in Applied Physics*, Vol. 12: *Turbulence* (P. Bradshaw, Ed.), Springer-Verlag, New York, 1978

79 Leschziner, M. A. Modeling turbulent recirculating flows by finite-volume methods—current status and future directions. *Int. J. Heat and Fluid Flow*, 1989, **10**, 186–202

80 Launder, B. E. Second-moment closure: Present ... and future? *Int. J. Heat and Fluid Flow*, 1989, **10**, 282–300

81 Elghobashi, S. E. and Abou Arab, T. W. A two-equation turbulence model for two-phase flows. *Physics of Fluids*, 1983, **26**, 931–938

82 Pourahmadi, F. and Humphrey, J. A. C. Modeling solid-fluid turbulent flows with application to predicting erosive wear. *Int. J. Phys. Chem. Hydro.*, 1983, **4**, 191–219

83 Schuh, M. J., Schuler, C. A., and Humphrey, J. A. C. Numerical calculation of two-phase flow and erosion in particle-laden gas flows past tubes. *AIChE J.*, 1989, **35**, 466–480

84 Torobin, L. B. and Gauvin, W. H. Fundamental aspects of solid-gas flow. *Can. J. Chem. Eng.*, 1959, **37**, 129, 167, 224

85 Torobin, L. B. and Gauvin, W. H. Fundamental aspects of solid-gas flow. *Can. J. Chem. Eng.*, 1960, **38**, 142, 189

86 Torobin, L. B. and Gauvin, W. H. Fundamental aspects of solid-gas flow. *Can. J. Chem. Eng.*, 1961, **39**, 113

87 Marble, F. E. Dynamics of a gas containing small solid particles. *Combustion and Propulsion*, 5th AGARD Colloquium, Pergamon Press, Oxford, 1963, 175–215

88 Marble, F. E. Mechanism of particle collision in the one-dimensional dynamics of gas-particle mixtures. *Physics of Fluids*, 1964, **7**, 1270–1282

89 Marble, F. E. Dynamics of dusty gases. *Ann. Rev. Fluid Mech.*, 1970, **2**, 397

90 Soo, S. L. *Fluid Mechanics of Multiphase Systems*, Blaisdell, London, 1967

91 Wallis, G. *One-Dimensional Two-Phase Flow*, McGraw-Hill, New York, 1969

92 Owen, P. R. Pneumatic transport. *J. Fluid Mech.*, 1969, **39**, 407–432

93 Hinze, J. O. *Turbulent Fluid and Particle Interaction*, Vol. 6: *Progress in Heat and Mass Transfer*, Pergamon Press, New York, 1972

94 Happel, J. and Brenner, H. *Low Reynolds Number Hydrodynamics*, 2nd ed., Noordhoff, Leyden, Netherlands, 1973

95 Batchelor, G. K. Transport properties of two-phase materials with random structure. *Ann. Rev. Fluid Mech.*, 1974, **6**, 227

96 Peskin, R. L. Some fundamental research problems in gas-solid flow. *AIChE Symposium Series*, 1975, **71**, No. 147, 52–59

97 Clift, R., Grace, J. R., and Weber, M. E. *Bubbles, Drops and Particles*, Academic Press, New York, 1978

98 Rudinger, G. Fundamentals of gas-particle flow. *Handbook of Powder Technology*, Vol. 2, (J. C. Williams and T. Allen, Eds.), Elsevier Scientific, Amsterdam, 1980

99 Di Giacinto, M., Sabetta, F., and Piva, R. Two-way coupling effects in dilute gas-particle flows. *J. Fluids Eng.*, 1982, **104**, 304–312

100 Drew, D. A. Mathematical modeling of two-phase flow. *Ann. Rev. Fluid Mech.*, 1983, **15**, 261–291

101 Jurewicz, J. T., Stock, D. E., and Crowe, C. T. The effect of turbulent diffusion on gas particle flow in an electric field. Thermal Energy Laboratory Report No. 77-6, Mechanical

Engineering Department, Washington State University, 1977
102 Shuen, J. S., Chen, L. D., and Faeth, G. M. Predictions of the structure of turbulent, particle-laden round jets. *AIAA J.*, 1983, **21**, 1483–1484
103 Shuen, J. S., Solomon, A. S. P., Zhang, Q. F., and Faeth, G. M. Structure of particle-laden jets: Measurements and predictions. *AIAA J.*, 1985, **23**, 396–404
104 Faeth, G. M. Recent advances in modeling particle transport properties and dispersion in turbulent flow. *Proc. ASME–JSME Thermal Eng. Joint Conf.*, Vol. 2, Honolulu, Hawaii, March 20–24, 1983
105 Yeung, W. S. Fundamentals of the particulate phase in a gas-solid mixture. Report No. LBL-8440, Lawrence Berkeley Laboratory, University of California, Berkeley, 1978
106 Abrahamson, J. Collision rates of small particles in vigorously turbulent fluid. *Chem. Eng. Sci.*, 1975, **30**, 1371–1379
107 Dukowicz, J. K. A particle-fluid numerical model for liquid sprays. *J. Comp. Physics*, 1980, **35**, 229–253
108 Lee, J. S. and Humphrey, J. A. C. Radiative-convective heat transfer in dilute particle-laden channel flows. *Int. J. PhysChem Hydro.*, 1986, **7**, 325–351
109 Doss, E. D. Analysis and application of solid-gas flow inside a venturi with particle interaction. *Int. J. Multiphase Flow*, 1985, **11**, 445–458
110 Gouesbet, G., Berlement, A., and Picart, A. Dispersion of discrete particles by continuous turbulent motions. Extensive discussion of the Tchen theory, using a two-parameter family of Lagrangian correlation functions. *Phys. Fluids*, 1984, **27**, 827–837
111 Goldschmidt, V. W., Householder, M. K., Ahmadi, G., and Chuang, S. C. Turbulent diffusion of small particles suspended in a turbulent jet. *Prog. Heat Mass Trans.*, 1972, **6**, 487–508
112 Lilly, G. P. Effect of particle size on particle eddy diffusivity. *Chem. Fundam.* 1973, **12**, 268–275
113 Peskin, R. L. and Kau, C. J. Numerical simulation of particle motion in turbulent gas-solid channel flow. *J. Fluids Eng.*, 1979, **101**, 9
114 Brown, D. J. and Hutchinson, P. The interaction of solid or liquid particles and turbulent fluid flow fields—A numerical simulation. *J. Fluids Eng.*, 1979, **101**, 265–269
115 Rizk, M. A. and Elghobashi, S. E. The motion of a spherical particle suspended in a turbulent flow near a plane wall. *Phys. Fluids*, 1985, **28**, 806–817
116 Chao, B. T. Turbulent transport behavior of small particles in dilute suspension. *Osterr. Ing. Arch.*, 1964, **18**, 7–21
117 Kreplin, H. P. and Eckelmann, H. Behavior of the three-fluctuating velocity components in the wall region of a turbulent channel flow. *Phys. Fluids*, 1979, **22**, 1233
118 Crowder, R. S., Daily, J. W., and Humphrey, J. A. C. Numerical calculation of particle dispersion in a turbulent mixing layer flow. *J. Pipelines*, 1984, **4**, 159–169
119 Abramovich, G. N. Effect of solid-particle or droplet admixture on the structure of a turbulent gas jet. *Int. J. Heat and Mass Transf.*, 1971, **14**, 1039–1045
120 Boothroyd, R. G. and Walton, P. J. Fully developed turbulent boundary-layer flow of a fine solid-particle gaseous suspension. *Ind. Eng. Chem. Fundam.*, 1973, **12**, 75–82
121 Zisselmar, R. and Molerus, O. Investigation of solid-liquid pipe flow with regard to turbulence modification. *Chem. Eng. J.*, 1979, **18**, 233–239
122 Crowe, C. T. Review—Numerical models for dilute gas-particle flows. *J. Fluid Eng.*, 1982, **104**, 297–303
123 Durst, F., Milojevic, D., and Schonung, B. Eulerian and lagrangian predictions of particulate two-phase flows: A numerical study. *Appl. Math. Modeling*, 1984, **8**, 101–116
124 Kallio, G. A. and Stock, D. E. Turbulent particle suspension: A comparison between lagrangian and eulerian model approaches. *Gas-Solid Flows—1986*, ASME FED-Vol. 35 (Library of Congress Catalog Card Number 83-73579), 1986
125 Hetsroni, G. Particles-turbulence interaction. *Proc. Third Int. Symp. on Liquid-Solid Flows*, ASME FED-Vol. 75 (Library of Congress Catalog Card Number 83-73577), 1988
126 Drew, A. D. Averaged field equations for two-phase media. *Studies in Applied Mathematics*, Vol. L, No. 2, Massachusetts Institute of Technology, 1971, 133–166
127 Drew, A. D. and Segel, L. A. Averaged equations for two-phase flows. *Studies in Applied Mathematics*, Vol. L, No. 3, Massachusetts Institute of Technology, 1971, 205–231
128 Whitaker, S. The transport equations for multi-phase systems. *Chem. Eng., Sc.*, 1973, **28**, 139–147
129 Sha, W. T. and Soo, S. L. Multidomain multiphase fluid mechanics. *Int. J. Heat and Mass Transf.*, 1978, **21**, 1581–1595
130 Hinze, J. O. Momentum and mechanical-energy balance equations for a flowing homogeneous suspension with slip between the two phases. *Appl. Sci. Res.*, Section A, 1962, **11**, 33–46
131 Murray, J. D. On the mathematics of fluidization. Part 1: Fundamental equations and wave propagation. *J. Fluid Mech.*, 1965, **2**, 465–493
132 Looney, M. L., Issa, R. I., Gosman, A. D., and Politis, S. Modelling of the turbulent flow of solid/liquid suspensions in stirred vessels. Presented at the 5th Int. Conf. on Mathematical Modelling, University of California, Berkeley, July 29–31, 1985
133 Taylor, G. I. Notes on possible equipment and technique for experiments on icing on aircraft. Aero. Res. Com., Rep. and Mem. No. 2024, 1940
134 Wenglarz, R. A. Boundary layer effects on impingement and erosion. *Proc. 17th Annual Cavitation and Poly-Phase Flow Forum*, ASME Fluids Eng. Conf., St. Louis, June 7–11, 1982
135 Boothroyd, R. G. *Flowing Gas-Solids Suspensions*, Chapman and Hall, London, 1971
136 Neilson, J. H. and Gilchrist, A. An analytical and experimental investigation of the velocities of particles entrained by the gas flow in nozzles. *J. Fluid Mech.*, 1968, **33**, 131–149
137 Menguturk, M. and Sverdrup, E. F. Calculated tolerance of a large electric utility gas turbine to erosion damage by coal ash particles. *Erosion: Prevention and Useful Applications*, (W. F. Adler, Ed.) ASTM STP 664, 1979, 193–224
138 Rodi, W. Examples of turbulence models for incompressible flows. *AIAA J.*, 1982, **20**, 872–879
139 Patel, V. C., Rodi, W., and Scheuerer, G. Turbulence models for near-wall and low Reynolds number flows: A Review. *AIAA J.*, 1985, **23**, 1308–1319
140 Kratina, P. and McMillan, J. Fly ash erosion in utility boilers—Prediction and protection. Combustion Engineering Power Systems, Report No. TIS-7309. Presented at the Can. Electr. Assoc. Conf., Regina, Saskatchewan, October 26–28, 1982
141 Reinhard, K. G. Turbine damage by solid particle erosion. Paper No. 76-JPGC-Pwr-15, IEEE-ASME Joint Power Gen. Conf., Buffalo, New York, September, 19–22, 1976
142 *Proc. 5th Int. Conf. on Erosion by Liquid and Solid Impact* (J. E. Field, Ed.), Cambridge, England, 1979
143 *Proc. 6th Int. Conf. on Erosion by Liquid and Solid Impact* (J. E. Field and N. S. Corney, Eds.), Cambridge, England, 1983
144 Tabakoff, W. and Hussein, M. F. Effect of suspended solid particles on the properties in cascade flow. *AIAA J.*, 1971, **9**, 1514–1519
145 Tabakoff, W. and Hussein, M. F. Pressure distribution on blades in cascade nozzle for particulate flow. *J. Aircraft*, 1971, **8**, 736–738
146 Tabakoff, W., Hosny, W. and Hamed, A. Effect of solid particles on turbine performance. *J. Eng. for Power*, 1976, **98**, 47–52
147 Hussein, M. F. and Tabakoff, W. Dynamic behavior of solid particles suspended by polluted flow in a turbine stage. *J. Aircraft*, 1973, **10**, 434–440
148 Hussein, M. F. and Tabakoff, W. Computation and plotting of solid particle flow in rotating cascades. *J. Computers and Fluids*, 1974, **2**, 1–15
149 Grant, G. and Tabakoff, W. Erosion prediction in turbomachinery resulting from environmental solid particles. *J. Aircraft*, 1975, **12**, 471–478
150 Hamed, A. Particle dynamics of inlet flow fields with swirling vanes. *J. Aircraft*, 1982, **19**, 707–712
151 Katsanis, T. and McNally, W. D. Revised FORTRAN program for calculating velocities and streamlines on the hub-shroud midchannel stream surface of an axial, radial or mixed flow turbomachine or annular duct: Vols. 1 and 2. NASA TN D8430 and NASA TN D8431, 1977
152 Beacher, B., Tabakoff, W., and Hamed, A. Improved particle trajectory calculations through turbomachinery affected by

coal ash particles. *J. Eng. for Power*, 1982, **104**, 64–68
153 Hamed, A. and Fowler, S. Erosion pattern for twisted blades by particle laden flows. *J. Eng. for Power*, 1983, **105**, 839–843
154 Wenglarz, R. A. and Menguturk, M. Use of cascade and small turbine tests to determine erosion of utility turbines. *J. Eng. for Power*, 1982, **104**, 58–63
155 Wenglarz, R. A. Erosion potential resulting from particulate flow in a multi-stage turbomachine. Report No. 83-2E3-FACTA-P1, Westinghouse R+D Center, Pittsburgh, 1983
156 Gunes, D. and Menguturk, M. Improved particle trajectory calculation around blade leading edge. *Proc. 6th Int. Conf. on Erosion by Liquid and Solid Impact*, Cambridge, England, 1983
157 Humphrey, J. A. C. Numerical calculation of developing laminar flow in pipes of arbitrary curvature radius. *Can. J. Chem. Eng.*, 1978, **56**, 151
158 Humphrey, J. A. C., Whitelaw, J. H., and Yee, G. Turbulent flow in a square duct with strong curvature. *J. Fluid Mech.*, 1981, **103**, 443–463
159 Chang, S. M., Humphrey, J. A. C., and Modavi, A. Turbulent flow in a strongly curved U-bend and downstream tangent of square cross-sections. *Int. J. PhysChem Hydro.*, 1983, **4**, 243–269
160 Iacovides, H. and Launder, B. E. The computation of momentum and heat transport in turbulent flow around pipe bends. Inst. Chem. Engrs. Symp. Series 86, 1st U.K. National Heat Transfer Conference, Leeds, July, 1984
161 Ghia, F. N., Mueller, T. J., and Patel, B. R. Computers in flow predictions and fluid dynamics experiments. ASME Winter Annual Meeting, Washington, D.C., Nov. 15–20, 1981 (Library of Congress Catalog Card Number 81-69010)
162 McNally, W. D. and Sockol, P. M. Review of computational methods for internal flows with emphasis on turbomachinery. *J. Fluids Eng.*, 1985, **107**, 6–22
163 Menguturk, M. and Sverdrup, E. F. A theory for fine particle deposition in 2-D boundary layer flows and application to gas turbines. Paper No. 81-GT-54, Gas Turbine Conf. and Prod. Show, Houston, March 9–12, 1981
164 Menguturk, M., Gunes, D., Mimaroglu, H. K., and Sverdrup, E. F. Blade boundary layer effects on turbine erosion and deposition. *J. Fluids Eng.*, 1983, **105**, 270–276
165 Mason, J. S. and Smith, B. V. The erosion of bends by pneumatically conveyed suspensions of abrasive particles. *Powder Tech.*, 1972, **6**, 323–335
166 Ulke, A. and Rouleau, W. T. The effects of secondary flows on turbine blade erosion. Paper No. 76-GT-74, Gas Turbine and Fluids Eng. Conf., New Orleans, March 21–25, 1976
167 Abdel Azim, A. F., Lasser, R., and Rouleau, W. T. Three-dimensional viscous particulate flow in a typical turboexpander. Paper presented at Int. Symp. on Modeling, Policy and Economics of Energy and Power Systems—Alternative Energy Sources and Technology (IASTED), Cambridge, Massachusetts, July 7–9, 1982
168 Abdel Azim, A. F. and Rouleau, W. T. Secondary flow effect on erosion damage of stationary cascade. *Proc. 6th Int. Conf. on Erosion by Liquid and Solid Impact*, Cambridge, England, 1983
169 El-Sayed, A. F. (Abdel Azim), Lasser, R., and Rouleau, W. T. Effects of secondary flow on particle motion and erosion in a stationary cascade. *Int. J. Heat and Fluid Flow* 1986, **7**, 146–154
170 Young, J. P. and Ruff, A. W. Particle erosion measurements on metals. *J. Eng. Mater. and Tech.*, 1977, **99**, 121–125
171 Wolak, J., Worm, P., Patterson, I., and Bodoia, J. Parameters affecting the velocity of particles in an abrasive jet. Paper no. 76-WA/Mat-6, ASME Winter Annual Meeting, New York, NY, December 5–10, 1976
172 Benchaita, M. T., Griffith, P., and Rabinowicz, E. Erosion of metallic plate by solid particles entrained in a liquid jet. *J. Eng. Ind.*, 1983, **105**, 215–227
173 Hashish, M. Cutting with abrasive waterjets. *Mech. Eng. J.*, March 1984, 60–69
174 Raask, E. Tube erosion by ash impaction. *Wear*, 1969, **13**, 301–315
175 Riley, J. J. and Patterson, G. S. Diffusion experiments with numerically integrated isotropic turbulence. *Phys. Fluids*, 1974, **83**, 529
176 McLaughlin, J. B. Aerosol particle deposition in numerically simulated channel flow. *Phys. Fluids*, 1989, **A1**, 1211–1224
177 Brauer, H. Report on investigations on particle movement in straight horizontal tubes, particle/wall collision and erosion of tubes and tube bends. *J. Powder and Bulk Solids Tech.*, 1989, **4**, 3–12
178 Hutchings, I. M., Macmillan, N. H., and Richerby, D. G. Further studies of the oblique impact of a hard sphere against a ductile solid. *Int. J. Mech. Sci.*, 1981, **23**, 639–646
179 Armstrong, J. D., Collings, N., and Shayler, P. J. Trajectory of particles rebounding off plane targets. *AIAA J.*, 1984, **22**, 214–218
180 Tilly, G. P. A two stage mechanism of ductile erosion. *Wear*, 1973, **23**, 87–96
181 Goodwin, J. E., Sage, W., and Tilly, G. P. Study of erosion by solid particles. Proc. Inst. Mech. Eng., 1969, **184**, Pt. 1, No. 15, 279–292
182 Chorin, A. J. Numerical study of slightly viscous flow. *J. Fluid Mech.*, 1973, **57**, 785–796
183 Schweitzer, M. and Humphrey, J. A. C. Note on the experimental measurement of particle flux to one and two in-line tubs. *Wear*, 1988, **126**, 211–218
184 Rubinow, S. I. and Keller, J. B. The transverse force on a spinning sphere moving in a viscous fluid. *J. Fluid Mech.*, 1961, **11**, 447–459
185 Saffman, P. G. The lift on a small sphere in a slow shear flow. *J. Fluid Mech.*, 1965, **22**, 385–400. (See also: Saffman, P. G. Correction. *J. Fluid Mech.*, 1968, **31**, 624.)
186 Lawler, M. and Lu, P. C. The role of lift in the radial migration of particles in pipe flow. *Advances in Solid-Liquid Flow in Pipes and Its Application* (I. Zandi, Ed.), Pergamon Press, Oxford, 1971, 39–57
187 Poe, G. G. and Acrivos, A. Closed-streamline flows past rotating single cylinders and spheres-inertia effects. *J. Fluid Mech.*, 1975, **72**, 605–623
188 Tsuji, Y., Morikawa, Y., and Mizuno, O. Experimental measurement of the Magnus force on a rotating sphere at low Reynolds numbers. *J. Fluids Eng.*, 1985, **107**, 484–488
189 Schlichting, H. *Boundary Layer Theory*, McGraw-Hill, New York, 1979
190 Reynolds, A. J. *Turbulent Flows in Engineering*, John Wiley and Sons, New York, 1974
191 Dennis, S. C. R., Singh, S. N., and Ignham, D. B. The steady flow due to a rotating sphere at low and moderate Reynolds numbers. *J. Fluid Mech.*, 1980, **101**, pp. 257–279
192 Schneider, P. J. Multiparticle erosion test facility. *Proc. 6th Int. Conf. on Erosion by Liquid and Solid Impact* (J. E. Field and N. S. Corney, Eds.), Cambridge, England, 1983, 66-1–66-9
193 Finnie, I. and Kabil, Y. H. On the formation of surface ripples during erosion. *Wear*, 1965, **8**, 60–69
194 Scattergood, R. O. and Routbort, J. L. Transient and synergetic effects erosion of silicon. *J. Am. Ceram. Soc.*, 1981, **64**(8), C-104–106
195 Gulden, M. E. Effect of number of impacts on erosion of polycrystalline MgF_2 in the elastic-plastic response regime. *J. Am. Ceram. Soc.*, 1980, **63**(3–4), 121–126
196 Rickerby, D. G. and Macmillan, N. H. The erosion of aluminum by solid particle impingement at normal incidence. *Wear*, 1980, **60**, 369–382
197 Bellman, R. and Levy, A. Erosion mechanism in ductile metals. *Wear*, 1981, **70**, 1–27
198 Brown, R., Jun, E. J., and Edington, J. W. Erosion of α-Fe by spherical glass particles. *Wear*, 1981, **70**, 347–363
199 Cantwell, Organized motion in turbulent flow. *Ann. Rev. Fluid Mech.*, 1981, **13**, 457–515
200 Fernholz, H.-H. External flows. *Topics in Applied Physics, Vol. 12: Turbulence* (P. Bradshaw, Ed.), Springer-Verlag, Berlin 1976, 45–107
201 Andrews, D. R. and Field, J. E. Temperature dependence of the impact response of copper: Erosion by melting. *J. Phys. D: Appl. Phys.*, 1982, **15**, 2357–2367
202 Hammartsen, A., Soderberg, S., and Hogmark, S. Study of erosion mechanisms by recovery and analysis of wear fragments. *Wear of Materials* (K. C. Ludema, Ed.), Book No. H00254, ASME, New York, 1983

203 Hutchings, I. M., Winters, R. E., and Fields, J. E. Solid particle erosion of metals—Removal of surface material by spherical projectiles. *Proc. Roy. Soc.*, 1976, **A348**, 379–392

204 Jennings, W. H., Head, W. J., and Manning, C. R. A mechanistic model for the prediction of ductile erosion. *Wear*, 1976, **40**, 93–112

205 Smeltzer, C. E., Gulden, M. E., and Compton, W. A. Mechanisms of metal removal by impacting dust particles. *J. of Basic Eng.*, 1970, **92**, 639–654

206 Shewmon, P. G. Mechanism of erosion of aluminum alloys. *Proc. 5th Int. Conf. on Erosion by Liquid and Solid Impact* (J. E. Field, Ed.), Cambridge, England, 1979

207 Tilly, G. P. Erosion caused by airborne particles. *Wear*, 1969, **14**, 63–79

208 Ganesan, P., Mehrotra, P. K., and Sargent, G. A. A microstructural study of the erosion/corrosion behavior of type 304 and 310 stainless steel. *Microstructural Science*, Vol. 10 (White, Richardson, McCall, Eds.), Elsevier Science, 1982

209 Hogmark, S., Hammarsten, A., and Soderberg, S. On the combined effects of corrosion and erosion. *Proc. 6th Int. Conf. on Erosion by Liquid and Solid Impact* Cambridge, England, 1983

210 Uhlig, H. H. *Corrosion and Corrosion Control*, John Wiley and Sons, New York, 1971

211 Scully, J. C. *The Fundamentals of Corrosion*, Pergamon Press, Oxford, England, 1975

212 Fontana, M. G. and Greene, N. D. *Corrosion Engineering*, McGraw-Hill, New York, 1978

213 Sedriks, A. J. *Corrosion of Stainless Steels*, John Wiley and Sons, New York, 1979

214 Pini, G. C., Bachmann, E., and Orkenyl, J. G. Errosion-corrosion tests at high velocity flows. *Mater. Perf.*, 1976, **15**, 37–38

215 Zambelli, G. and Levy, A. V. Particulate erosion of NiO scales. *Wear*, 1981, **68**, 305–331

216 Maasberg, J. A. and Levy, A. V. Erosion of elevated-temperature corrosion scales on metal. *Wear*, 1981, **73**, 355–370

217 Levy, A. V. and Slamovich, E. Combined corrosion-erosion of steels in oxidizing environments. Report No. LBL-15657, Materials and Molecular Research Division, Lawrence Berkeley Laboratory, University of California, Berkeley, 1984

218 Ives, L. K. Erosion of 310 stainless steel at 975°C in combustion gas atmospheres. *J. Eng. Mater. Tech.*, April 1977, 126–132

219 Ives, L. K., Young, J. P., and Ruff, A. W. Particle erosion measurements on metals at elevated temperatures. Proceedings of the 24th Meeting of the Mechanical Failures Prevention Group, April 1976, 145–158

220 Ruff, A. W., Young, J. P., and Ives, L. K. Erosion measurements on metals at elevated temperatures. Proceedings of the 2nd Int. Conf. on Mech. Behavior of Materials, August 1976, 1989–1993

221 Kang, C. T., Chang, S. L., Birks, N., and Pettit, F. S. Erosion-corrosion of coatings and super alloys in high velocity hot gases. *Proc. 3rd J.I.M. Int. Conf. on High Temp. Corrosion of Metals*, Japan, 1982